ABSTRACT

Thesis: COLD TESTING OF A RADIAL EXTRACTION OUTPUT CAVITY FOR A FREQUENCY DOUBLING GYROKLYSTRON

Karthik Bharathan, Masters of Science, 2004

Thesis Directed By: Professor Wesley G. Lawson, Department of Electrical and Computer Engineering

Research in the University of Maryland Gyroklystron program has centered around the development of a 17.136 GHz gyroklystron, that combines the gyrotron mechanism with the ballistic bunching of klystrons to produce a high power, high gain amplifier. The current tube is a 4-cavity (input, buncher, penultimate and output) coaxial, frequency doubling system that will be used as a driver for the Haimson Research Corporation (HRC) accelerator structure. This thesis presents the design, simulation, optimization, cold test methodology and performance data of a proposed radial extraction output cavity in which the microwave energy is extracted through an inner coaxial conductor in the TE_{01} circular mode. The positioning of dielectrics in the drift spaces and the effect of axial and radial misalignments between the inner and outer walls of the cavity were studied at depth and quantified. One advantage of this topology is that it reduces the size and complexity of the output waveguide chain otherwise needed to convert the TE_{02} circular mode from the gyroklystron into the standard rectangular waveguide for injection into the HRC accelerator structure. Cold

test results show that this new cavity, which has a Q of 458 and a resonant frequency of 17.112 GHz, is a viable replacement for the output cavity currently in the system, as long as the cavity is well-aligned.

COLD TESTING OF A RADIAL EXTRACTION OUTPUT CAVITY FOR A FREQUENCY DOUBLING GYROKLYSTRON

By

Karthik Bharathan.

Thesis submitted to the Faculty of the Graduate School of the
University of Maryland, College Park, in partial fulfillment
of the requirements for the degree of
Master of Science
2004

Advisory Committee:

Professor Wesley G. Lawson, Chair
Professor Victor L. Granatstein
Professor Patrick G. O' Shea

Acknowledgements

I'm eternally grateful to my advisors Prof. Wes Lawson, and Prof. Victor Granatstein for giving me the opportunity to work on the IREAP - Gyroklystron Program at the University of Maryland. Throughout the course of my research, Prof. Lawson's proficiency with the theoretical and experimental aspects of the program, served as a primary resource to overcome obstacles I'd encountered. Prof. Granatstein provided invaluable assistance in helping me select a balanced course load with an emphasis on Electrophysics, which would lay a sound foundation for my research.

I thank Bart Hogan for giving me a glimpse of the skills one could pick up with a mechanical engineering background or simply as someone who was willing to learn on the job, and striving to achieve perfection.

Emmanuel Gouveia, who patiently went over the procedures and practices for operating lab equipment, running simulations, purchasing, inventory control, and who's breadth of knowledge on the program as well as unrelated topics never fails to amaze me.

The administrative staff at IREAP, Nancy Boone, Carol Bellamy, Dorothea Brosius who gave me a sense of belonging to a group, and never just a number on payroll.

The unquestioning support of my parents and family who gave me this opportunity to pursue my Masters at the University of Maryland, and who were with me every step of the way, from half a world away.

Table of Contents

List of Tables

List of Figures

Chapter 1: Introduction

1.1 Overview

This thesis deals with the design and cold testing of a radial extraction output cavity, as one of the future system upgrades for the University of Maryland Gyroklystron (GKL) program-conducted at the Institute for Research in Electronics and Applied Physics (IREAP). This work is organized in a sequence of four chapters. The first gives an overview of the current status of the GKL program, its primary and allied research areas. The second chapter deals with the motivation behind the design of the new output cavity and its simulated performance. The third is the crux of the thesis, which deals with the cold test methodology and data obtained from the testing of the cavity. Anomalies encountered are modeled and resimulated, and correlation between the experimental results and theoretical performance is highlighted in the final chapter, making a strong case for the use of this cavity in a future system.

1.2 University of Maryland Gyroklystron Program

Traditionally the microwave amplifier of choice for driving high-energy linear electron accelerators has been the klystron. To push the limits of high-energy physics, electron-positron colliders with center of mass energies in excess of 1 TeV would be required [1]. Hundreds or thousands of klystrons would need to be cascaded together to power the next-generation colliders, so phase control along with peak power and efficiency, would be important parameters in determining the system performance. A prerequisite to their development would be the improvement of the technology of

pulsed microwave amplifiers with regards to their efficiency, reliability and the ability to provide peak power in excess of the current state-of-the-art. The 100 GeV Stanford Linear Collider represents the current linear collider standard for which a 1 μs, 150 MW, S-Band klystron was developed. However the power train for future linear colliders would need to operate in X-band or above, and obtaining comparable powers from the klystron would be non-trivial as their peak power scales with the square of the output wavelength [2].

Thus, research at the University of Maryland GKL program has centered around the development of a 17.136 GHz (six times the current SLAC frequency) gyroklystron, that combines the gyrotron mechanism with the ballistic bunching of klystrons to produce a high power, high gain amplifier. Significant milestones recently achieved in the project include a 3-cavity first harmonic coaxial system, which produced over 75 MW of peak power at 8.57 GHz, and a 3-cavity, frequency-doubling system that produced 27 MW at 17.14 GHz. The latter served as a starting point for the design of a 4-cavity frequency doubling system [3] that was expected to have a large-signal gain of above 50 dB. This was achieved in part by the introduction of an additional gain cavity (penultimate cavity) before the output cavity. A preliminary experimental study of this tube showed it to have an efficiency of 7 % and a gain of 23.3 dB. The highest peak power observed was 18.5 MW [8]. The discrepancy between the predicted performance and the experimental results is attributed in part to the presence of an instability in the input cavity, which forces the gyroklystron to be operated with velocity pitch ratio (α) values significantly below the design value of

1.4. This reduction in α is mainly due to a non-uniformity in the azimuthal distribution of beam current due to a faulty emitter design.

The current focus of the experiment is to condition the 4-cavity system to act as a driver for the accelerator structure designed and delivered to the University of Maryland by the Haimson Research Corporation (HRC) [4]. This resulted in a number of experimental tasks that were simultaneously initiated to collectively serve as a system overhaul and upgrade. They included: (a) redesign of the input cavity to overcome the instabilities observed in the preliminary testing, (b) modification of the output section of the tube to increase TE_{02} mode purity from 96 % to over 99.9 %, (c) replacement of the faulty emitter with a unit having reduced temperature and work function variations-optionally replacing the electron gun assembly completely with an improved design from Calabazas Creek Research Co., (d) design of an emitter testing/processing station (TERP Station-Thermionic Emitter Research & Processing) to characterize emitter performance in-house, (e) investigation of a radial power extraction scheme from the output cavity of the system, and (f) increasing gain of the 4 – cavity tube to about 60 dB, which would allow the use of a TWT amplifier and solid state source to provide the input, thus enabling feed forward techniques to be incorporated to reduce phase variation of the gyroklystron output.

1.3 Gyroklystron Test Facility

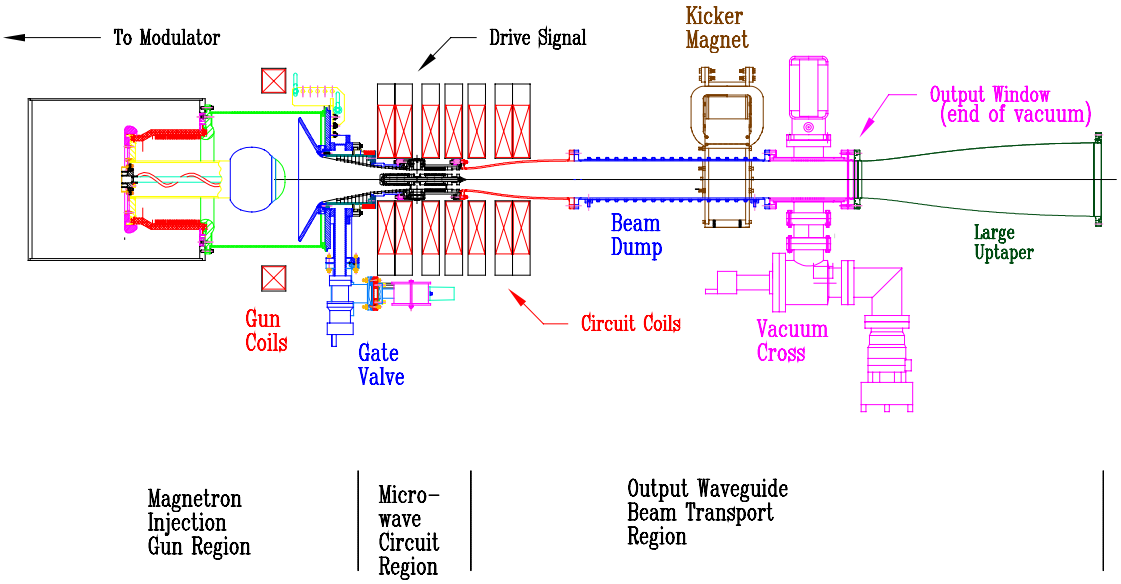

Figure 1-1: Gyroklystron test facility layout.

Figure 1-1 is a schematic of the test facility where the different gyroklystron tubes are tested and characterized. The modulator is mainly comprised of a high voltage switching supply, the Lambda-EMI 802L - a 50 kV capacitive charging supply, pulse forming networks (PFNs), high voltage thyratron switches and a high voltage pulse transformer. It can support 100 MW tubes, with a single anode Magnetron Injection Gun (MIG), producing 500 kV, 500 A pulses of 1 μs duration at a rep rate of 5 Hz. The system uses a single anode MIG, which is driven by the modulator and emits an annular beam of electrons and rated at a beam current between 480-720 A, with an axial velocity spread less than 7 % [7]. Under the influence of an external magnetic field set by the gun coils, the electrons undergo rotational motion about their equilibrium positions, and the beam is compressed adiabatically to an α of about 1.5. Excluding the gun magnet, there are 7 solenoidal, water-cooled pancake magnets,

which are capable of producing magnetic fields in excess of 0.5 T. The magnetic compression at the entrance to the microwave circuit is mainly influenced by the gun coil. Three independent power supplies that feed the pancake magnets can be adjusted to get the desired field shape or slope in the circuit. The input power for the gyroklystron is provided by a mechanically tunable (8.47 GHz – 8.70 GHz) coaxial magnetron built by Varian. It's capable of putting out 2-2.5 μs pulses with a peak power of 150 kW. This drive signal is injected in the input cavity to initiate beam bunching in the microwave circuit. Beam transport is achieved via a downtaper that connects the gate valve on the MIG front to the microwave circuit. Beyond this region is the beam dump, where the electron beam is exhausted by striking against the walls of the waveguide. This section is water cooled and provided with lead shielding for heat dissipation and X-ray absorption, respectively. A kicker magnet at the end of the beam dump, rated at 800 G, ensures that any remaining stray electrons in the beam are forced against the waveguide walls. The amplified microwave signal, separated from the electron beam now exits the system through an alumina window, which serves to separate the ultra-high vacuum of the system from the atmospheric pressure downstream section hereon. The waves then travel through a large uptaper before being fed to an anechoic chamber for diagnostics.

1.4 Interfacing the UM gyroklystron with HRC accelerator structure

The HRC accelerator structure employs a compact power multiplier system based on a dual hybrid feed (TE_{10} rectangular mode) bridge configuration, effectively generating high accelerating gradients [4]. To enable the experimental system to be a driver for the HRC accelerator structure, a power transport system that connects the output of the gyroklystron (TE_{02} circular mode) to the two rectangular WR-62 injection arms of the HRC structure was designed and fabricated (Fig. 1-2).

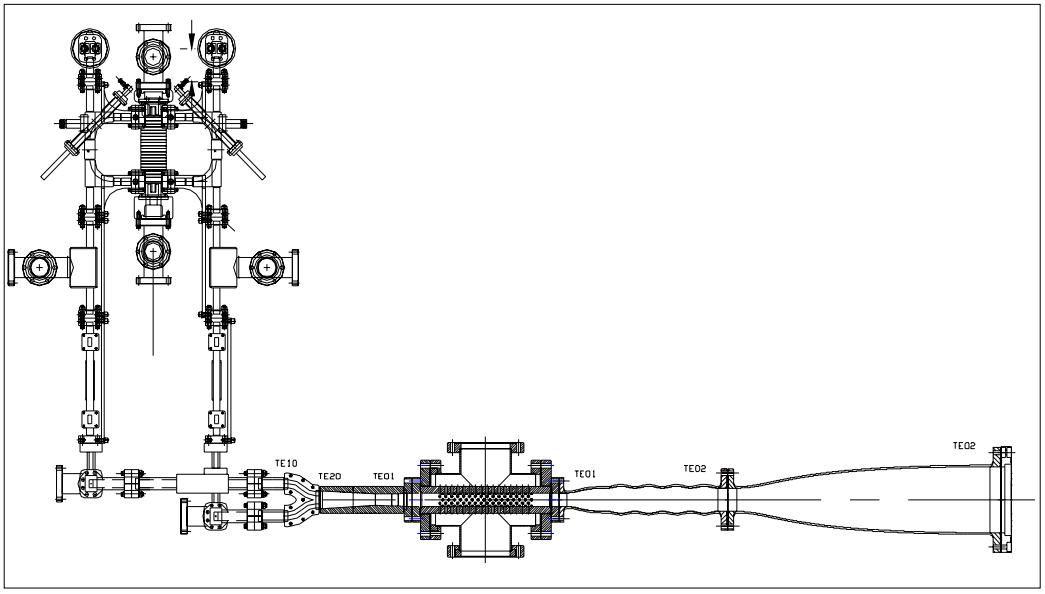

Figure 1-2: Power transport from UM gyroklystron to HRC accelerator structure.

The output signal from the large uptaper (which would ordinarily feed the anechoic chamber) is now diverted via a non-linear downtaper to a ripple wall mode converter that converts the TE_{02} circular mode into the TE_{01} circular mode. It then passes

through a pumping cross before entering a compact TE_{01} circular to TE_{20} rectangular mode converter [5]. A bifurcation then divides the power equally between the two injection arms by converting the TE_{20} rectangular mode into a TE_{10} rectangular mode in each arm. E and H plane bends are used to orient the drive signal for the HRC accelerator structure, and a phase shifter is provided for phase equalization of the signals in the dual feed arms.

Chapter 2: Theoretical studies of the radial extraction output cavity

2.1 Motivation for radial extraction scheme

A common feature of various gyroklystron amplifiers, differing in their operating frequency, number and geometric profile of their cavities, cavity modes and harmonic number, is the axial microwave power extraction scheme. In this scheme the amplified microwave signal and the spent electron beam travel together in the output waveguide, where a beam dump dissipates the remaining electron energy. Optionally, a depressed collector could be employed to recover the energy and feed it back into the system in order to improve the system efficiency. In these schemes the cross section of the output waveguide differs slightly from the cross section of the output cavity and undergoes a gradual variation over an axial distance of several wavelengths. In this region of the microwave circuit, the electron beam energy is as yet unexhausted with essentially the same beam cross section, and remains potentially well-coupled to the operating mode or various spurious modes. Thus, reverse energy transfer from the microwaves to the electron beam, which significantly reduces the efficiency of the system, is possible.

Zero-drive instability is a condition in which a significant amount of output power is generated even in the absence of a drive signal. Without a drive signal to initiate bunching, the beam quality remains very high. The large reduction in the output waveguide dimensions prior to injecting into the accelerator structure increase the likelihood of trapped modes in the tapered sections. Reflections may occur in the output waveguide or at the window, when downtapering pushes propagating modes below cutoff. A long non-linear tapered waveguide section could act as a cavity or as a backward wave oscillator, with a low start oscillation condition. Thus a power extraction scheme in which the downtapering of the output waveguide is minimized will have improved zero-drive stability.

The level of excitation of the output cavity fields from the a.c. signal is much greater than that in the input, buncher and penultimate cavities. This, compounded with the fluctuations in the cross section of the output waveguide system, raises concerns of high-localized electric fields, which could cause electric field breakdown or heat dissipation problems. The axial extraction scheme also necessitates a ripple wall mode converter section downstream to convert the TE_{02} coaxial mode from the gyroklystron into the TE_{01} circular mode, which is the desired output mode for accelerator applications that require pulse compression. Such a design would involve a tradeoff between bandwidth and mode purity, in addition to compensating for any spurious modes generated in the chain [6].

Thus, an improved extraction scheme would provide for a method to separate the microwaves from the spent beam rapidly, while simultaneously ensuring that the signal is extracted from the output cavity in a mode that minimizes the need to

significantly reduce the output waveguide dimensions and enable the system to be zero drive stable.

With this background, the concept of a radial extraction output cavity was developed as a viable alternative to the current axial extraction system for the gyroklystron amplifier. The original design was proposed by James Anderson [7], and the model was further developed by E.S.Gouveia et al [8].

2.2 Current output cavity design

As illustrated in Figs. 2-1 and 2-2, the output cavity currently employed in the gyroklystron system is of the axial power extraction type, which operates in the TE_{021} mode. Experimentally the cavity was found to have a resonant frequency of 17.115 GHz and a Q of 310. The drift region which precedes this cavity on its upstream boundary, serves to cut off the TE_{021} mode. The downstream section of the cavity has a stepped-lip, which in addition to setting the diffractive Q of the cavity also serves to maximize the microwave power transmission in the desired mode and minimize mode conversion into the TE_{011} mode.

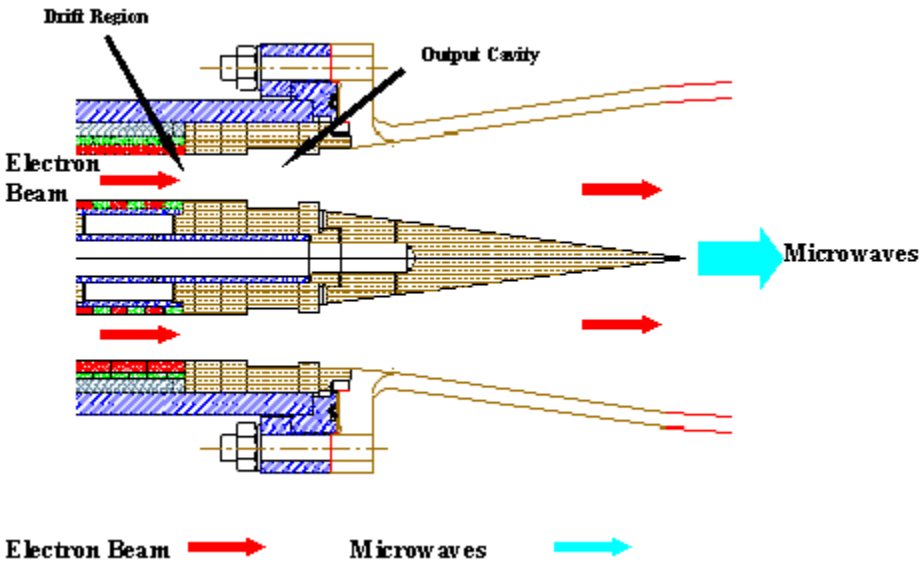

Figure 2-1: Typical axial-extraction output cavity.

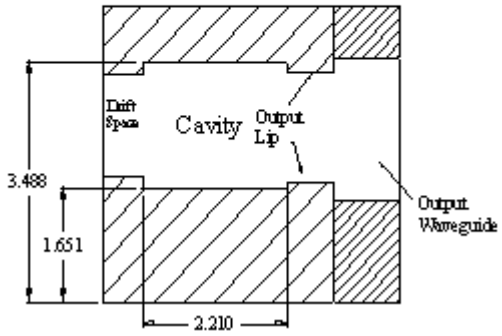

Figure 2-2: Detailed cross-sectional view of output cavity.

Figure 2-3 shows the set of dual tapers (comprised of an inner taper and an outer taper) that are employed to convert the TE_{02} coaxial mode emerging from the output cavity into the TE_{02} circular mode. The tapers were optimized [9] to reduce the mode conversion of the TE_{02} to less than 0.2%, and offer a theoretical normalized power

transmission of 98.9%. As a consequence of this arrangement, the microwave power and the spent electron beam travel concurrently along the tube axis where the beam is exhausted in the beam dump. The microwaves pass through a ceramic window, which serves as the demarcation point separating the ultra high vacuum system upstream from the waveguide and mode converter sections downstream. The amplified signal in the TE_{02} circular mode is then injected into an anechoic chamber for power measurements, mode purity and radiation pattern studies.

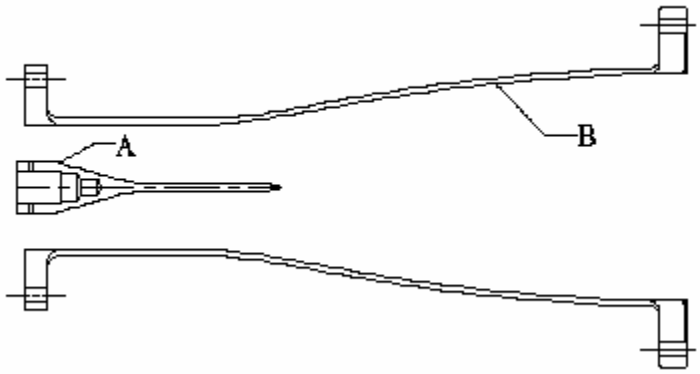

Figure 2-3: Current coax-circular mode conversion hardware. A - Inner Transition, B – Outer Taper.

2.3 Radial extraction output cavity

As seen in Fig. 2-4, the radial extraction output cavity is defined by changes in the radii of both the inner and outer walls. Strong axial magnetic fields at the inner and outer conducting walls are a characteristic of the TE_{021} coaxial mode that is excited in the output cavity. This mode is magnetically coupled to the TE_{01} coaxial mode in the

inner coax guide through four coupling slots symmetrically distributed about its azimuth. The E-field goes to zero at the metal boundaries. The inner coaxial structure terminates with a variable short on the upstream side. A conical coaxial to cylindrical transition on the downstream end, converts the coaxial TE_{01} mode generated in the inner cavity into the TE_{01} circular mode which is transported through the output waveguide system. The upstream and downstream boundaries of the cavity are occupied by drift regions that are cut off to the TE_{021} mode.

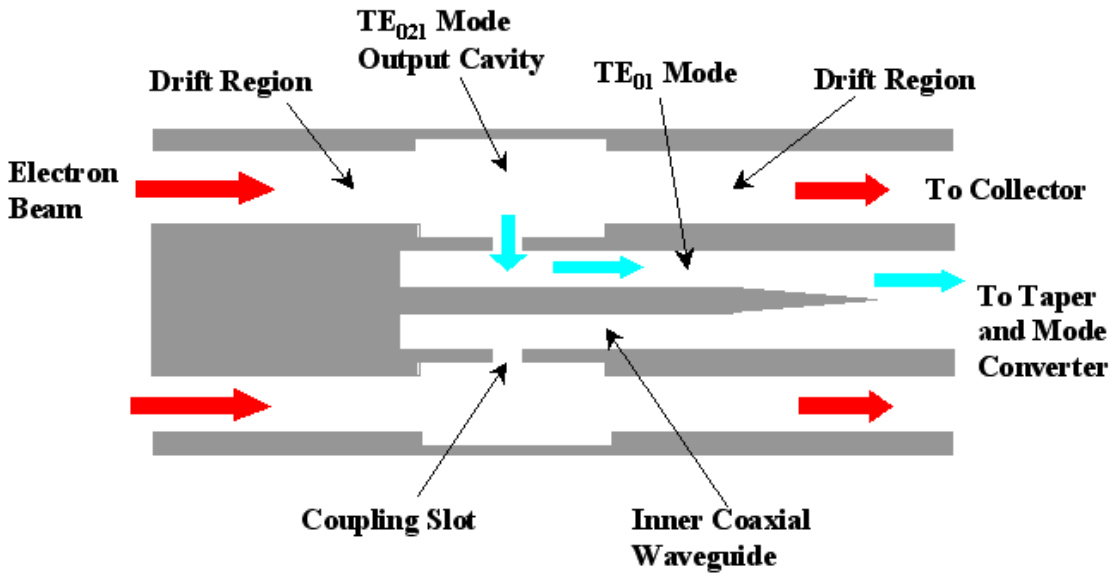

Figure 2-4: Schematic of proposed radial extraction output cavity.

The principal dimensions of the radial extraction output cavity are essentially the same as that for the conventional axial extraction output cavity present in the tube, as seen from Table 2-1. Additionally, the new cavity would have essentially the same gain and efficiency as the existing output cavity. As the tube has been optimized taking into account the parameters of the input, buncher, penultimate and output

cavities, even a slight change in the electromagnetic attributes, such as the resonant frequency or quality factor of a cavity might necessitate rework of the entire tube. The physical dimensions of the new cavity need to be comparable to that of the current one to ensure that the tube can be housed in its original assembly (vacuum jacket and related hardware) without a major overhaul of the circuit.

Output Cavity	New	Old
Outer Radius (cm)	3.530	3.488
Inner Radius (cm)	1.690	1.651
Axial Length (cm)	2.000	2.210
Drift Tube Radii		
Inner Radius	1.825	1.825
Outer Radius	3.325	3.325
Inner Coaxial Guide		
Outer Radius (cm)	1.460	N/A
Conical Taper Radius (cm)	0.480	N/A
Coupling Apertures		
Number	4	N/A
Axial Length (cm)	0.508	N/A

Angular Width (degrees)	81.5	N/A
Lip Dimensions		
Lip Width (cm)	N/A	0.693
Lip Height (cm)	N/A	0.100

Table 2-1: Structural comparison of new and old output cavities

2.4 Interfacing scheme with proposed radial extraction output cavity

The current interfacing scheme involves a power transport system in which the output waveguide is tapered down from a radius of 7.62 cm to a radius of 1.328 cm suitable for injection into the compact TE_{01} circular to TE_{20} rectangular (Tantawi) mode converter. Additionally this section must include the TE_{02} circular to TE_{01} circular mode ripple wall converter. The chief concern while designing tapered sections and mode converters are reflections and excitation of spurious modes that could affect system stability and performance [6]. In the proposed radial extraction output cavity, the microwave energy is magnetically coupled from the cavity via coupling slots into the inner conductor of a much smaller radius (1.46 cm) in the TE_{01} coaxial mode. The conical taper, which has a radius of 0.48 cm, progressively converts this mode into the TE_{01} circular mode further downstream. The volume of this waveguide is comparable to that of the Tantawi converter, thus avoiding the need for a long problematic down-taper scheme. It would also obviate the need for the ripple wall mode converter section, and improve the zero-drive capability of the system.

2.5 HFSS design of output cavity

The principle dimensions of the current axial extraction output cavity (obtained with GYCOAX and MAGYKL codes) served as the starting point for the radial extraction cavity design. The simulation package chosen was Ansoft's High Frequency Structure Simulator (HFSS)- a 3D, electromagnetic, finite-element simulation tool for high frequency design [14]. As seen in Fig. 2-5, a 3D model of the cavity is generated using a combination of the standard geometrical shapes available in the toolkit.

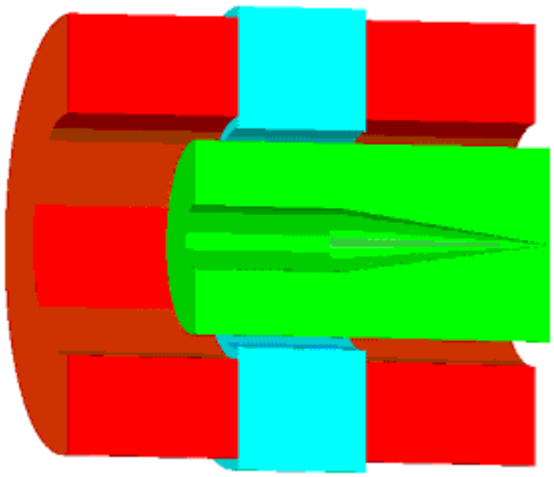

Figure 2-5: 3-D HFSS model of new output cavity (180 degree slice).

By taking advantage of cylindrical symmetery, a 90 degree slice of the HFSS model is constructed which requires the simulation of only one probing/injection port, the symmetery cuts defined as perfect electric boundaries. However the variable short in

the upstream section of the inner coax makes the system asymmetric in the Z-direction, necessitating a simulation of its complete axial length. Figure 2-6 is a simplified sectional diagram illustrating the individual parts of the output cavity. Section 1 in this figure is a WR-62 waveguide that is used to inject a drive signal or for diagnostics in the cold test piece.

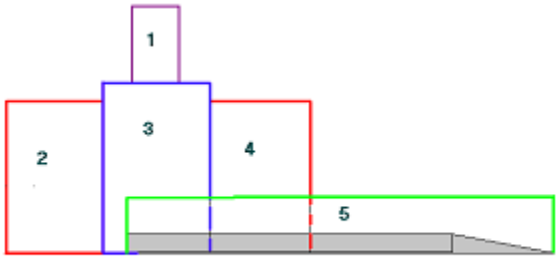

Figure 2-6: Simplified cross-sectional view of model. 1 - Injection Port, 2 -Upstream Drift Region, 3 – Output Cavity, 4 – Downstream Drift Region, 5 – Inner Guide for Power Extraction.

HFSS evaluates the cold test performance of the cavity by simulating the injection of a signal at the drive frequency through the WR-62 waveguide, which excites the TE_{021} mode in the cavity. This in turn generates the TE_{01} coaxial mode in the inner conductor. A mid-plane (z=0) cross sectional cut illustrates the electric field patterns (Fig. 2-7) that exist in the structure. The double radial variation field pattern of the TE_{021} coaxial mode is evident in the outer cavity region while the single radial variation field pattern of the TE_{01} coaxial mode shows up in the inner coax. Note the lack of azimuthal variation indicating that it is a circular electric (TE_{0n}) mode.

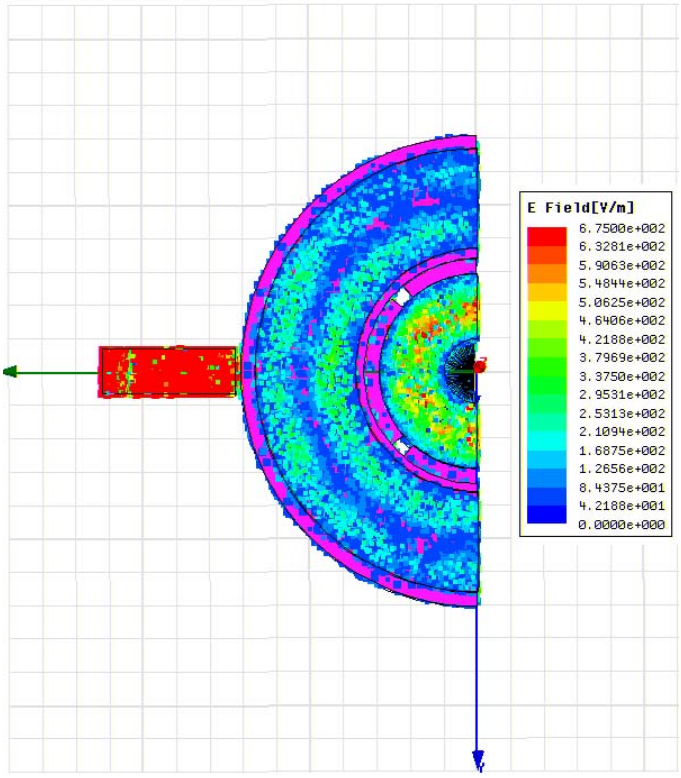

Figure 2-7: Mid-plane slice showing electric field distribution across cavity structure.

Figure 2-8 is a longitudinal slice along the axis of symmetry indicating the power transport taking place in the cavity and the penetration of fields in the drift regions (which is minimal). The addition of lossy dielectric materials in the drift regions would reduce this penetration further.

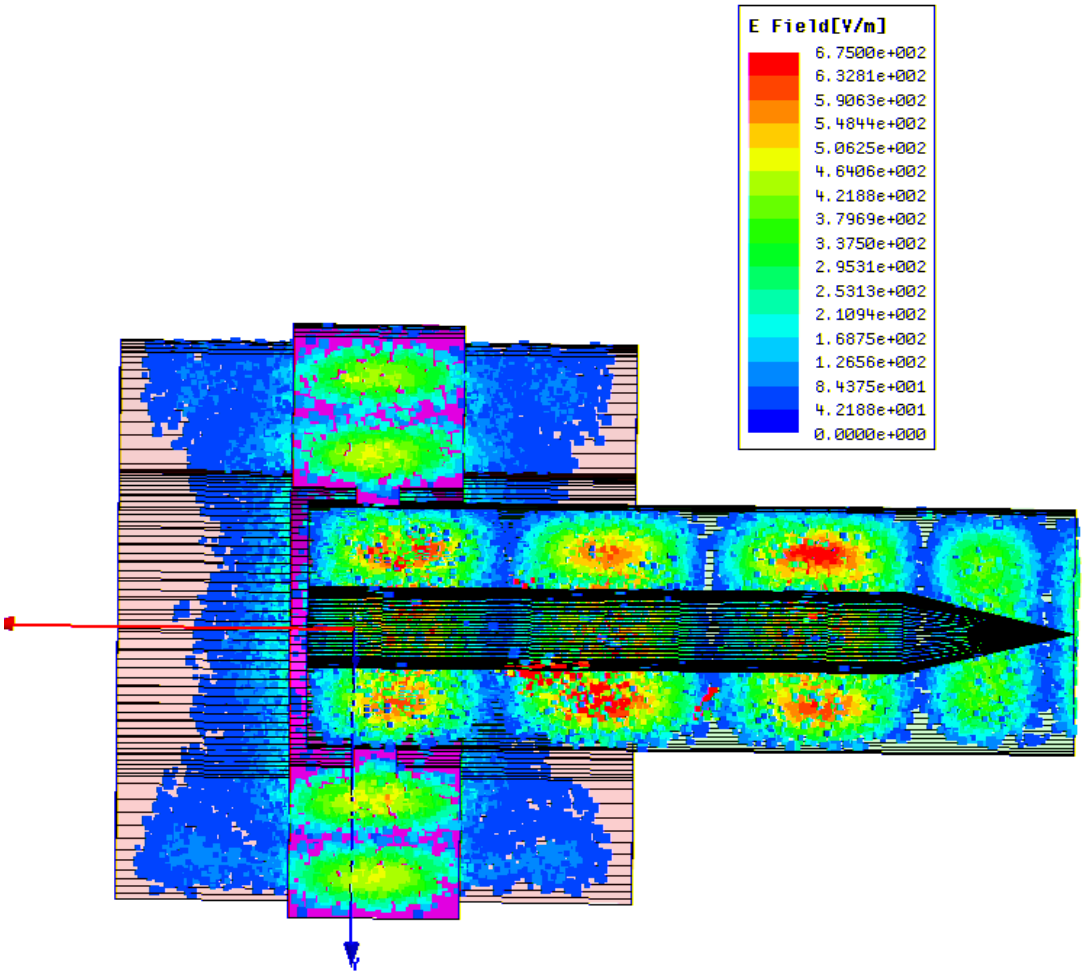

Figure 2-8: Longitudinal slice showing power transport in cavity structure

The design was optimized by variation of several parameters [7,8]. The primary ones being: the angular width and axial length of the coupling slots, the number of slots, the axial position of the variable short, the thickness of the inner wall of the output cavity. The coupling slots were the most sensitive and difficult element to design, as they greatly influence the resonant frequency and quality factor of the cavity. Figure 2-8 shows the simulated (HFSS) variation of Q and resonant frequency as a function of the axial length of coupling slots [8].

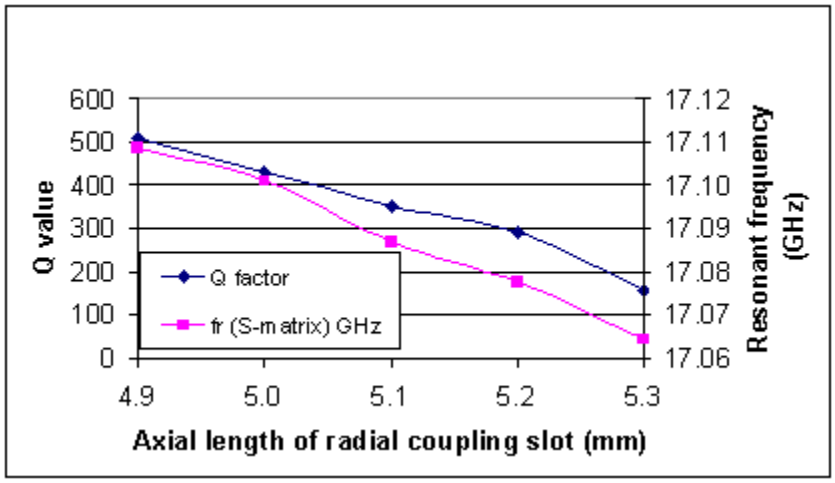

Figure 2-9: HFSS simulated Q and Resonant frequency variation vs. axial length of coupling slots.

The Q is particularly sensitive to fluctuations in slot length, varying by a factor of 10 for a slot length change of roughly 0.5 cm. However the cavity characteristics are not as sensitive to the azimuthal positioning of the slots as compared to their axial length sensitivity (which will be verified by simulations and experimental results in chapter 3). Another constraint was to make the metal conducting gaps between the slots as large as necessary to ensure mechanical strength of the system. The final optimized design called for 4 slots each having an angular width of 81.5 degrees, with an axial length of 5.08 mm. The simulated electromagnetic properties of the new output cavity are summarized in Table 2-2, which also compares the same with those of the output cavity currently utilized by the system. Figure 2-10 is the HFSS simulated S_{21} transmission curve for the cavity.

	New output cavity	Old output cavity
Resonant frequency (GHz)	17.08	17.115
Quality factor (Q)	354	310

Table 2-2: Electromagnetic property comparison of output cavities.

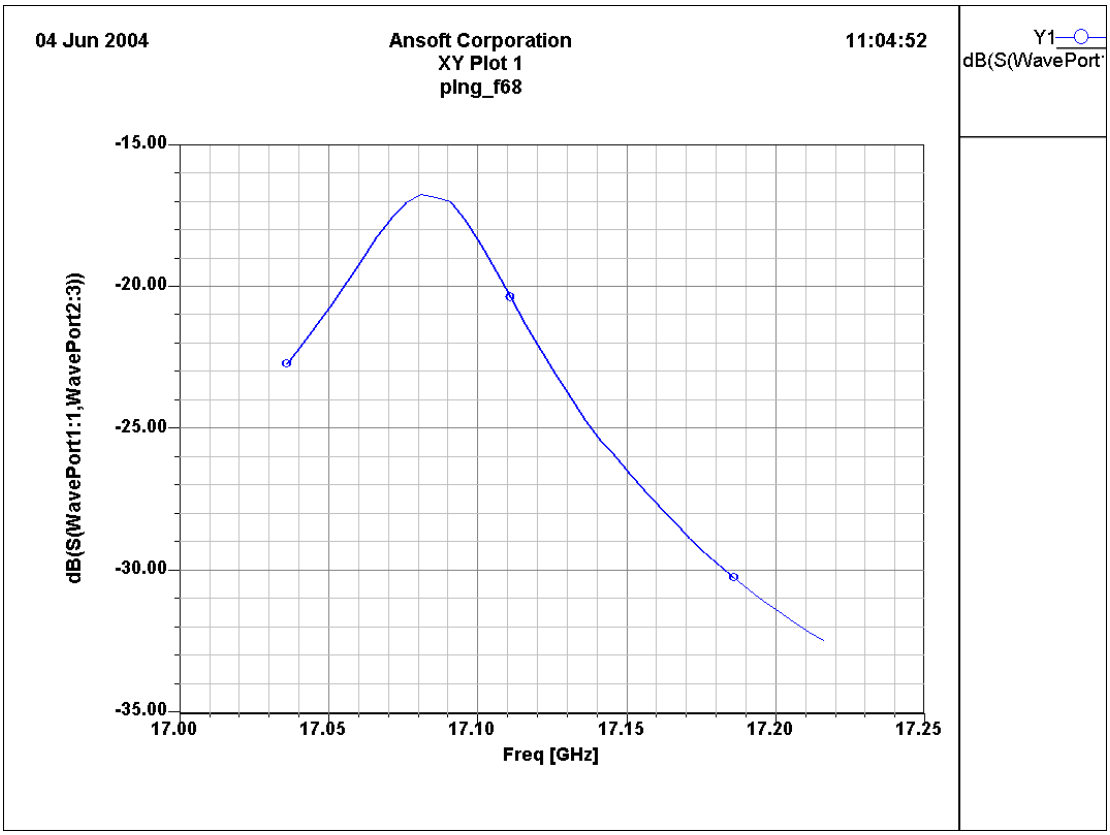

Figure 2-10: Theoretical S_{21} transmission curve with peak at ~17.08 GHz.

Chapter 3: Cold testing of radial extraction output cavity

3.1 Cavity test housing

The cavity is positioned at the center of a 150 mm long cylindrical support structure (Fig. 3-1) with an outer diameter of 112 mm and a thickness of 13 mm. Two cylindrical inserts, which also constitute the cutoff sections upstream and downstream, fit snugly into the outer housing. The upstream cylindrical insert has a 2 cm wide stepped lip, which actually forms the outer wall of the cavity. Each cutoff section, which doubles up as the drift section for the electron beam, is 6.4 cm long. Two small coupling apertures (1.02 mm x 3.81 mm) spaced 90 degrees apart are machined in the outer wall of the cavity, along with a press-fit arrangement for a WR-62 section of waveguide. The waveguide breaches through an opening in the outer housing, following which a waveguide to coax adapter can be attached for launching power (input port) or for diagnostics.

Figure 3-1: Output cavity test housing, with Dolph Chebychev taper and WR-62 injection arm.

A central cylinder with a radius of 1.46 cm forms the inner coax. It is supported by a corresponding depression in the faceplate of the outer housing in the downstream section, and terminated by a variable short in the upstream region. The axial position of the variable short is precisely controlled by a micrometer mechanism housed in the upstream faceplate of the outer housing. Radially, the section is aligned by moving within the confines of the inner coax. The 2 cm wide region of reduced cross section in the central part of the inner coax (which constitutes the inner wall of the cavity) is aligned with the stepped lip of the upstream insert, to effectively give the cavity an outer radius of 3.53 cm and an inner radius of 1.69 cm. Four azimuthal coupling slots are machined in this inner wall of the cavity, each having an angular width of 81.5 degrees. A 10 cm Dolph-Chebychev taper couples the output of the system to the TE_{01} mode filter/Marié converter. This unusual arrangement of an outer housing and cylindrical inserts was designed to permit testing of coaxial cavities with varying

radial dimensions as well as inner coaxial structures differing with respect to the size and number of coupling slots. The individual components of the test housing are shown in Fig. 3-2.

Figure 3-2: Exploded view of test housing-from left: inner coax, upstream and downstream inserts, micrometer variable short.

3.2 Marié converter

The output from the Dolph-Chebychev taper would ideally feed into the Marié converter (Fig. 3-3), which accepts the TE_{01} circular mode and converts it into the TE_{10} rectangular mode.

Figure 3-3: Ku-band Marié converter built by AFC Corp.

However the Marié converter is inherently a difficult component to model and fabricate as it lacks azimuthal symmetry, and its use in a previous set of experiments had led us to believe that it introduces spurious TE_{11},TE_{21} and TE_{31} (generally TE_{x1}) components and perhaps other nonsymmetrical modes when injected in the rectangular port [6]. To overcome this phenomenon, a TE_{01} mode filter was designed using fiberglass resistance cards wedged in a cylindrical housing that could be bolted on between the Dolph-Chebychev taper and the Marié converter section downstream.

3.3 TE_{01} mode filter

The filter housing (Fig. 3-4) consists of a 5 inch cylindrical aluminum section with an inner diameter of 4.216 cm, and a bolt pattern which matches that of the Marié converter rotatible flange.

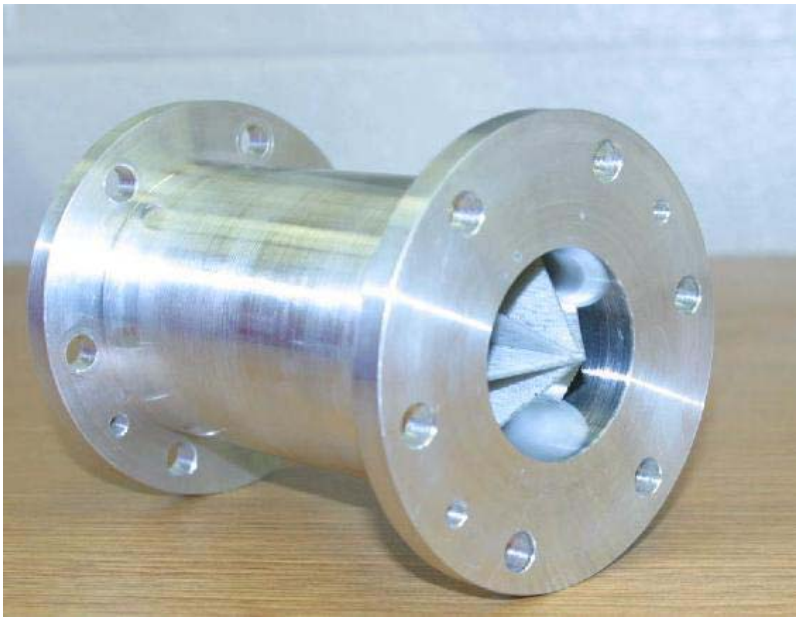

Figure 3-4: TE_{01} mode filter section.

Wedged symmetrically in this housing are 3 fiberglass resistance cards, which are 0.0812 cm thick, forming a 6-fin filter section. The base substrate for the card is a fine weave glass cloth impregnated with high temperature thermosetting resin. A resistive film of Nickel/Chromium is uniformly deposited on the substrate surface, approximately 50 millionths of an inch thick. A clear protective acrylic coating is provided over the metal film. The resistivity of 377 ohms per square was chosen to be close to the intrinsic impedance of free space. To minimize reflections from the obstruction the filter would ordinarily provide, 45 degree tapers were cut at both ends of each of the 3 cards. The composite system, including the filter and Marié converter, was tested to determine losses in the filter section that would need to be accounted for in the transmission curves.

3.4 Loss estimation in filter section

The test setup involves two stages. In the first stage the input signal from a scalar network analyzer is fed to a WR-62 variable attenuator via a 20 dB cross guide directional coupler, which samples the input power (channel B). The output from the variable attenuator (channel A) is changed by adjusting the position of the attenuating pad until the ratio of A/B is as close to zero as possible. Practically it was set to – 0.07dB. The pad is now locked in position to retain the attenuation setting, and the A/B reading is stored in the network analyzer memory. In the second stage, the circular filter section is sandwiched between 2 identical Marié converters, fed at one end via the 20 dB cross guide coupler and the output signal is taken from the 2nd Marié converter after passing through the attenuator (channel A). Assuming the loss in the Marié converter sections is negligible as compared to that in the filter, the difference between the new A/B reading and the memory, gives the loss in the filter section. Experimentally this was observed to be -2.70 dB.

3.5 Lossy material

The output cavity currently employed in the gyroklystron has its outer and inner radii as 3.488 cm and 1.651 cm respectively, which allow for sufficient beam clearance. This geometry however results in several modes that exist below the drive frequency that are not cutoff. In order to suppress these modes the drift regions are lined with

microwave-absorbing ceramics of two types: CIAS-carbon impregnated alumio – silicate and 80% BeO/20% SiC. Two layers of lossy ceramics are placed along the outer conductor in the drift region preceeding the output cavity. The outer layer is BeO-SiC and the inner layer is CIAS. The rings on the inner conductor alternate between BeO-SiC and CIAS [10,11].

Initial testing of the cavity Q and resonant frequency was conducted without loading the drift regions with lossy materials. This leads to interaction of spurious modes and reflections from the walls of the inserts, causing sharp spikes at local resonances in the transmission curve. To overcome this, the drift regions were loaded with Eccosorb BSR-II/SS-6M [12], a high-loss, ultra-thin (0.01 inch) elastomeric microwave absorber. This dielectric loading would closely approximate the BeO-SiC/CIAS rings used in the gyroklystron tube. BSR-II is a thin flexible, electrically non-conductive silicone rubber sheet, which can be cut with a knife and can be fitted to compound curves. The main characteristics of Eccosorb BSR-II are summarized in Tables 3-1 and 3-2. It is engineered to reduce or eliminate surface currents, cavity resonance, coupling, and generally dampen reflections. SS-6M variant has a pressure sensitive adhesive backing to the BSR-II, which lends itself easily to application on the inner walls of the inserts.

Frequency range	10-25 GHz
Volume resistivity, ohm-cm	2×10^8
Dielectric strength, volts/mil	>10

Table 3-1: Material characteristics of Eccosorb BSR-II.

Frequency (GHz)	5	10	18	25
Attenuation (dB/cm)	20	55	95	115

Table 3-2: Typical attenuation properties calculated from complex permittivity and complex permeability [12].

3.6 Data acquisition and scalar network analyzer setup

The HP8757C scalar network analyzer is the primary piece of equipment employed for cold testing of the cavity parameters. Power to the test setup is nominally 10 dBm, swept over the test range-centered at 17.136 GHz with a bandwidth of 600 MHz, and fed through a coax to WR-62 waveguide adapter. From here the signal travels through a cascade of 2 cross guide couplers. The first (30 dB) cross guide coupler is used to sample the input signal, and is measured by channel R of the scalar network analyzer. This value serves as the normalization factor for the reflected and transmitted signals from the cavity. The second (20 dB) cross guide coupler is flipped in orientation with respect to the first in the sense that it measures reflected power from the cavity. This is picked up by channel A of the network analyzer via a detector. From this point the signal proceeds to the Marié converter, the TE_{01} filter, Dolph-Chebychev taper, and finally to the cavity housing. Channel B connects to the radial extraction arm of the cavity to record the transmission profile of the signal exiting the cavity. This testing configuration is referred to as the axial injection, radial extraction topology (Fig. 3-5). Another variation introduced is one in which the signal in injected radially into the

cavity and extracted axially to study the cavity parameters. Both approaches however possess similar transmission characteristics, with variation only in the magnitude of reflection coefficient observed at the injection port, the value in the radial injection scheme being significantly larger due to the small coupling aperture.

Data acquisition, i.e., trace downloading was done using a software utility designed by Elisra Electronic Systems Ltd., Microwave Division [13]. The software mimics the response of a conventional HP plotter and grabs the graphical information sent to it from the HP8757C. Physically the information is downloaded through a GPIB cable that connects the HP-IB bus of the HP8757C and a PC fitted with a National Instruments PCI-GPIB card. In addition to maintaining a soft copy of the readout, this system offers additional advantages like plotting several graphs over each other (multi-trace), annotating results, and the ability to save and load into HPGL files or save in a bitmap format.

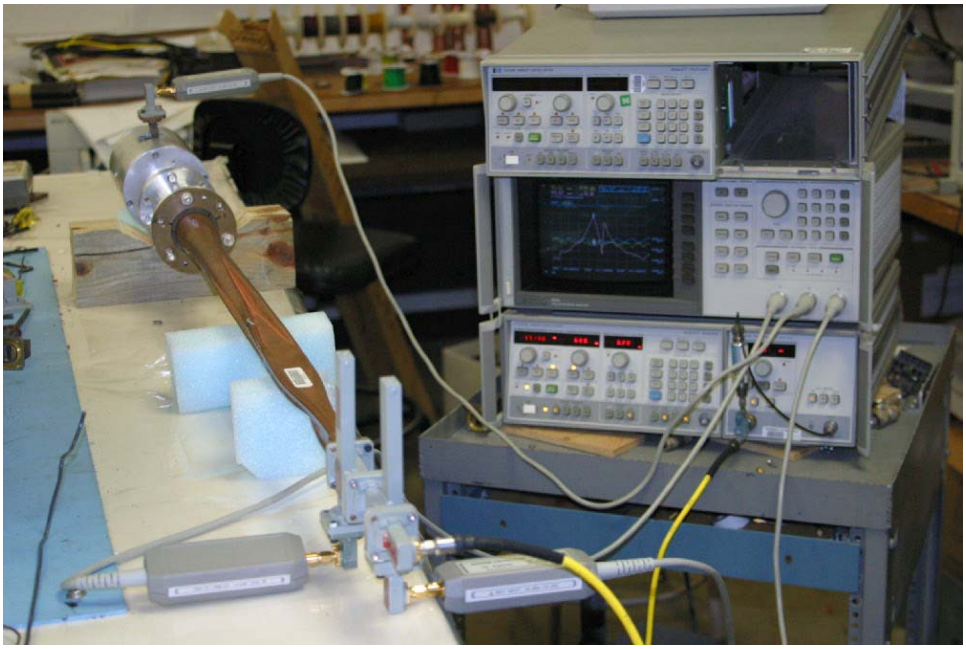

Figure 3-5: Complete cold test bench setup connected to HP8757C scalar network analyzer.

3.7 Test configuration #1-Lossy material present till cavity lip

In this test configuration the BSR-II strips were applied along the inner walls of the inserts upstream and downstream, till the cavity lip. The coupling slots were initially kept open (Fig. 3-6) and progressively closed (Fig. 3-7 to Fig. 3-10) with adhesive backed copper tape to study the variation of Q and resonant frequency as a function of slot length, to fine tune the cavity. The results are summarized in Table 3-3 and Fig. 3-11. As predicted by HFSS, the resonant frequency and Q rise with the decrease in coupling slot length. The X axis which represents the axial coupling slot length in

Fig. 2.9 ranges from 4.9 mm to 5.3 mm, while that in Fig. 3-11 ranges from 0 mm (slots closed) to 5.08 mm (slots 100% open). With a slot length of 5.08 mm, HFSS predicts a Q of 390 and a resonant frequency of 17.09 GHz, which is reasonably close to the experimentally observed Q of 356 and a resonant frequency of 17.04 GHz. A closer agreement between the theoretical and experimental readings is observed with the lossy material backed up from the cavity lip, as will be seen in section 3.8.

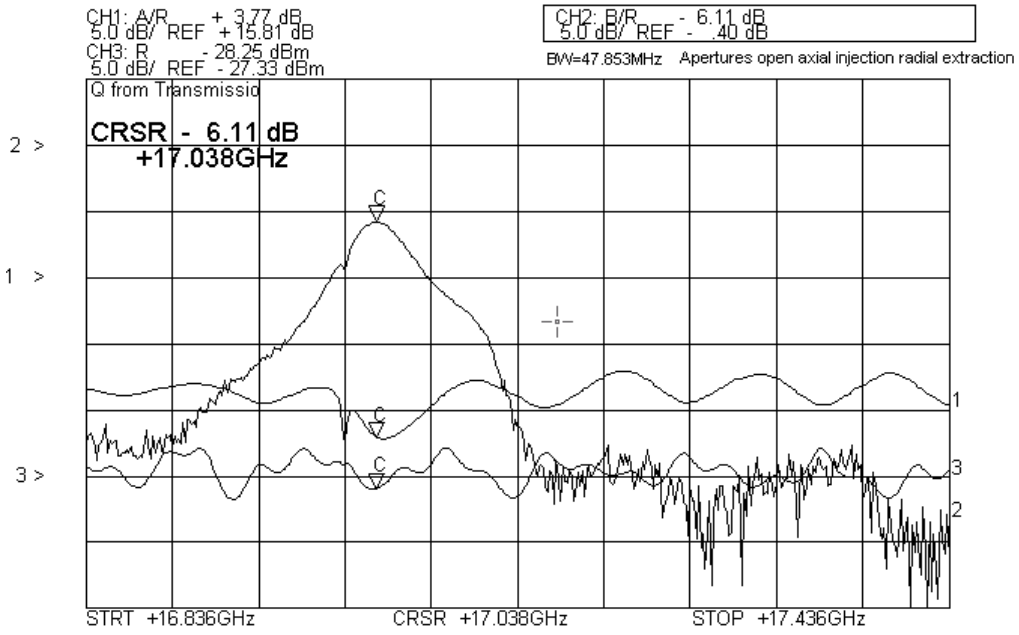

Figure 3-6: S_{21} transmission curve with all coupling slots open.

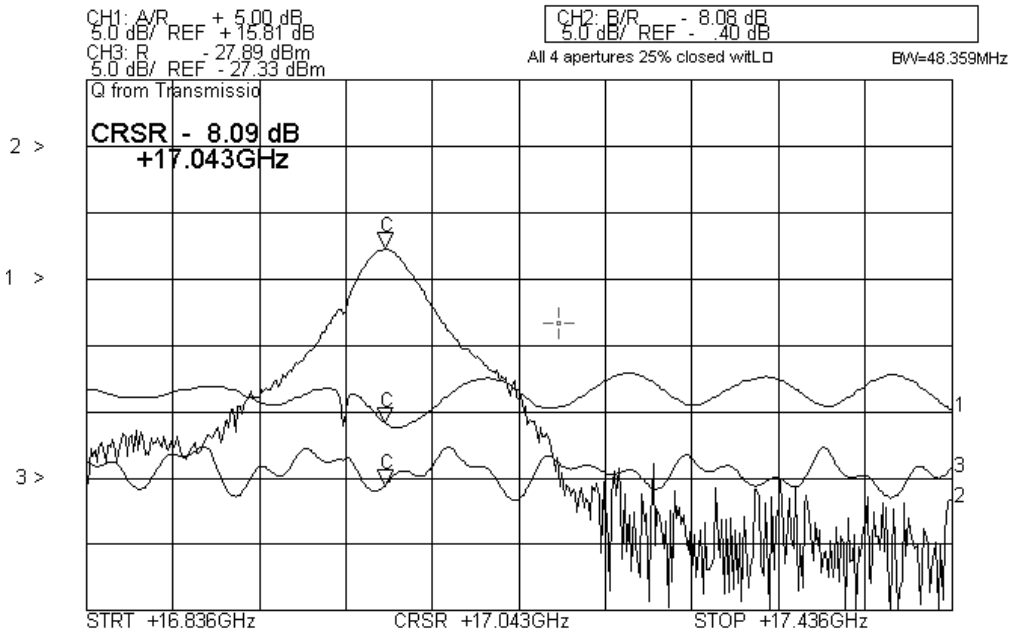

Figure 3-7: S_{21} transmission curve with coupling slots open 75%.

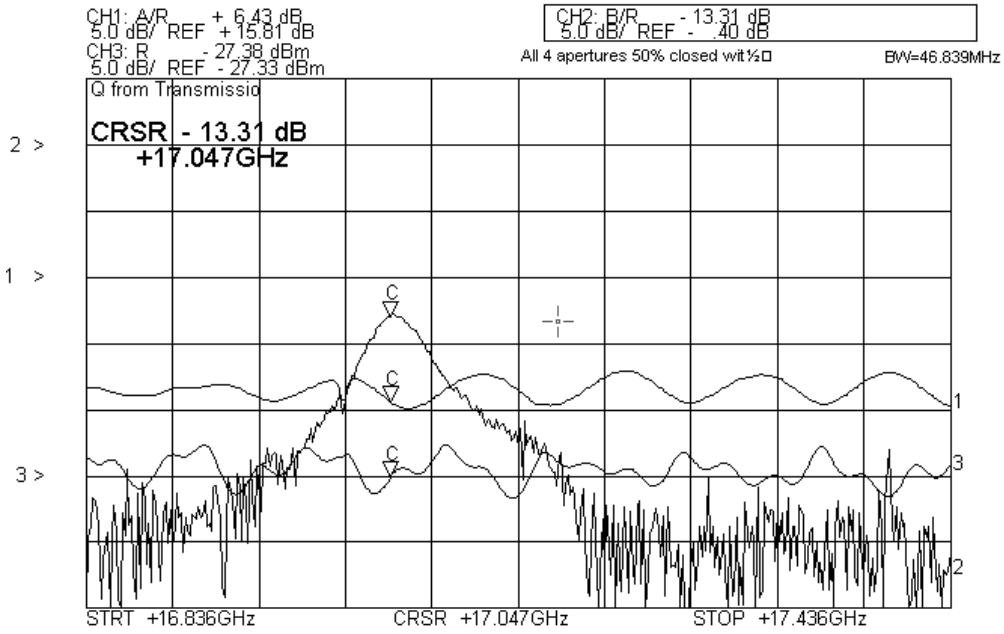

Figure 3-8: S_{21} transmission curve with all coupling slots open 50%.

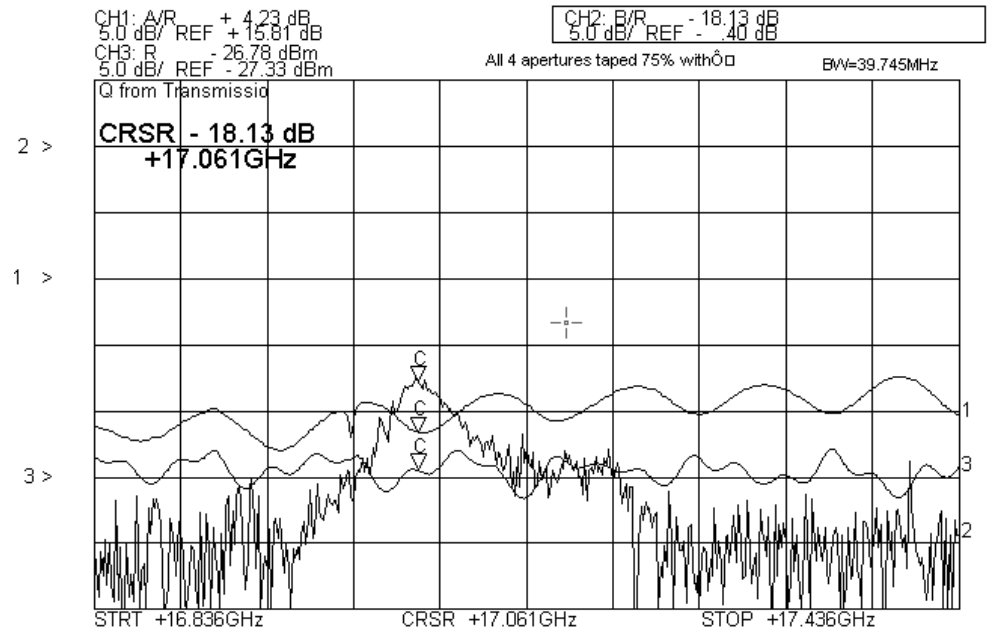

Figure 3-9: S_{21} transmission curve with all coupling slots open 25%.

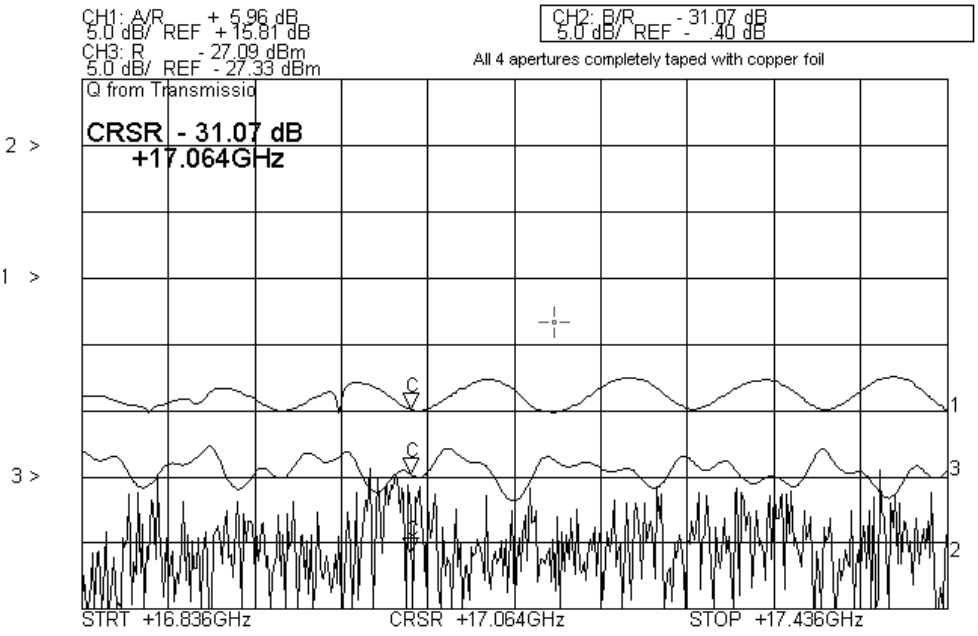

Figure 3-10: S_{21} transmission curve with coupling slots closed.

Inner Coax Coupling Slot Opening (%)	Resonant Frequency (GHz)	Quality Factor Q	Bandwidth (MHz)	Transmission Peak (dB)
100	17.038	356.05	47.853	-36.11
75	17.043	352.43	48.359	-38.09
50	17.047	363.95	46.839	-43.31
25	17.061	429.26	39.745	-48.13
0	-	-	-	-61.07

Table 3-3: Variation of transmission parameters as a function of inner coax coupling slot opening.

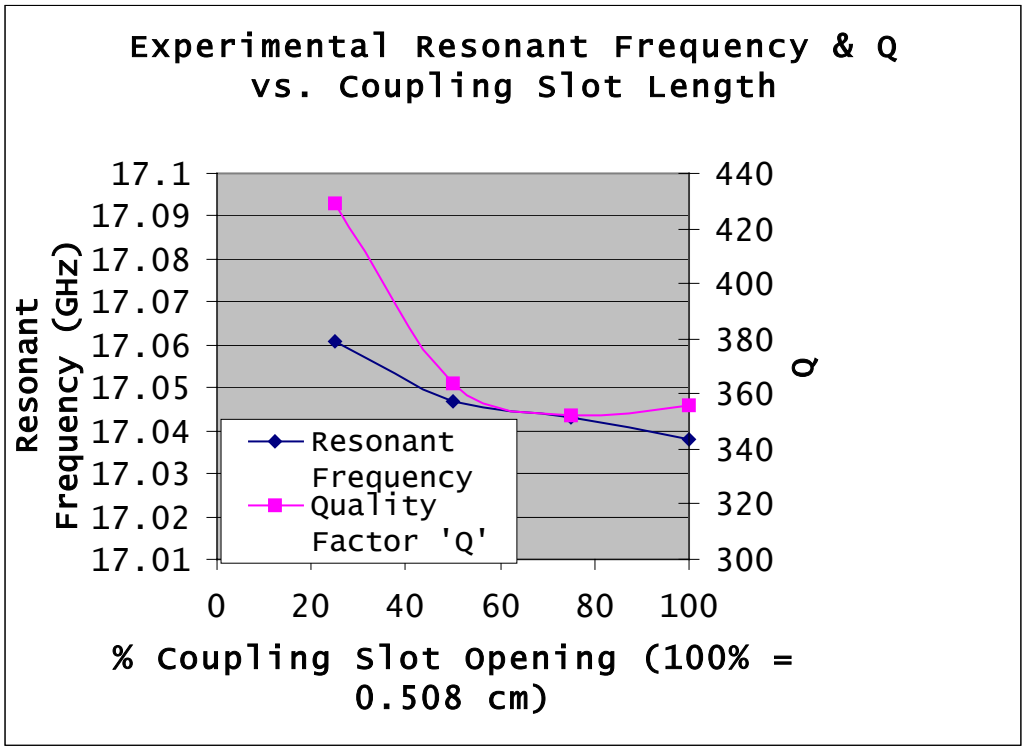

Figure 3-11: Variation of resonant frequency and Q as a function of slot length. Both Q and resonant frequency rise as the coupling slot length decreases.

3.8 Effect of radial injection and axial extraction

For the experimental setup described the cavity is essentially a reciprocal device. Power can be injected axially through the Marié converter and extracted radially through the side arm, or vice versa. The main difference in these two arrangements is that the reflected power level (CH1-A/R) in the latter case increases by 6.87 dB (Fig. 3-12) as compared to the former. This is attributed to the small dimensions of the coupling aperture in the outer wall of the cavity into which the radial arm feeds.

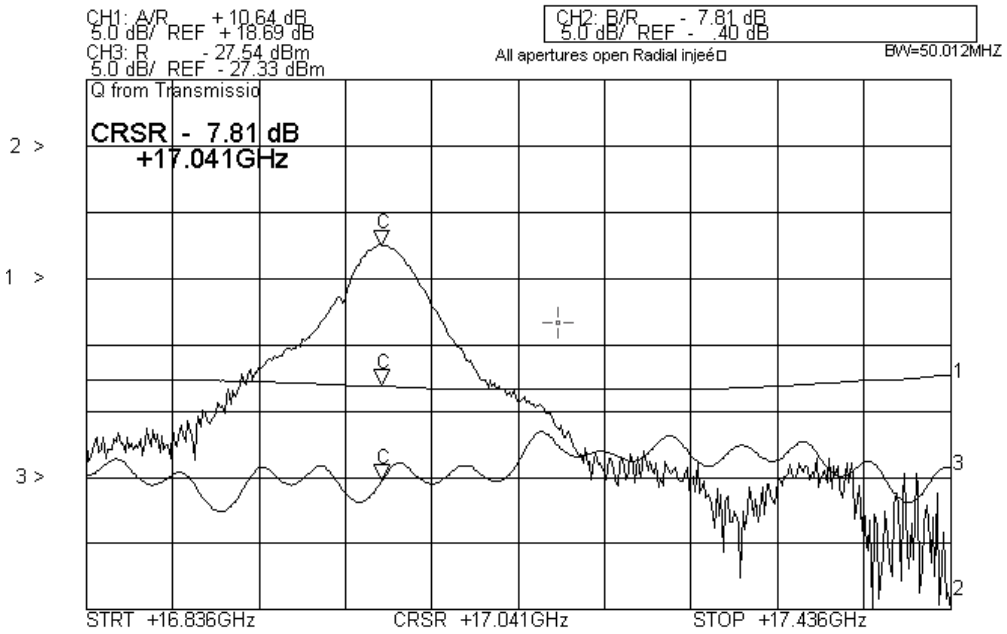

Figure 3-12: Transmission curve for Radial injection / Axial extraction topology.

3.9 Test configuration #2-lossy material backed up from cavity lip

In the previous test configuration, the lossy material was applied all the way till the cavity lip, in the drift sections. However this could have led to the suppression of some cavity modes in addition to increasing the losses in the cavity, lowering its Q. With a view to mimic the positioning of lossy materials in the drift region relative to the cavity lip in the present tube's output cavity, the BSR-II was backed off by 1.35 cm in the upstream and downstream drift regions. This would provide a more realistic scenario under which the transmission properties of the cavity could be studied. Experimentally it was observed (Fig. 3-13) that the S_{21} transmission curve which exhibited a single hump feature with the lossy material present till the cavity lip, now degenerates into 2 sharp humps staggered in frequency by 85 MHz, with different quality factors.

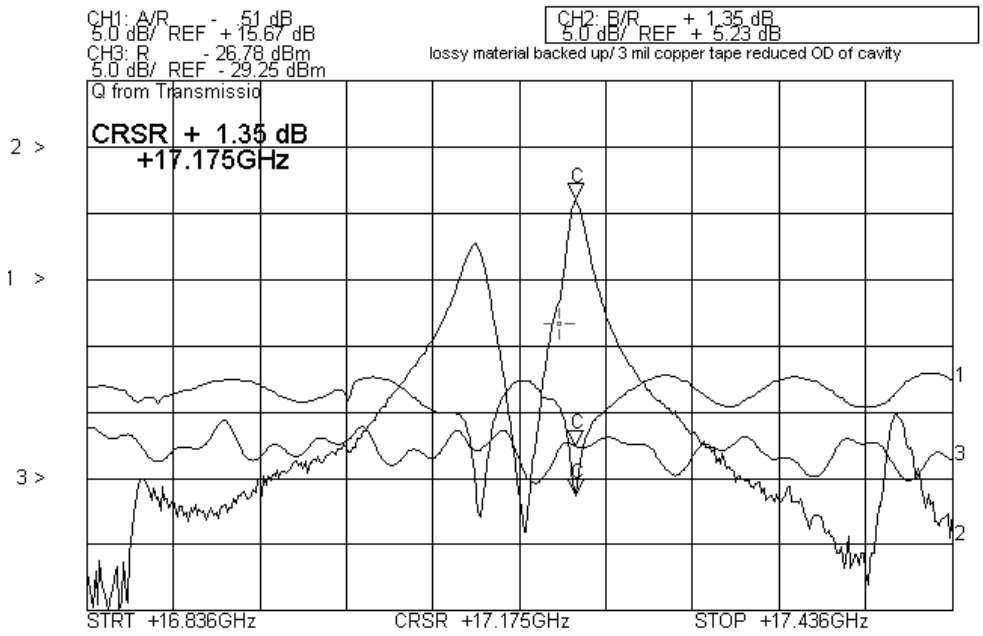

Figure 3-13 S_{21} Transmission curve with lossy material backed up 1.35 cm from cavity lip (upstream and downstream).

3.10 Fourier analysis of transmission curves

In order to theoretically model the dual resonant peaks observed, a Fourier analysis leading to a curve fit was carried out. Originally a single frequency curve fit was attempted. The electric field variation as a function of time can be represented in terms of an amplitude factor 'A', an exponentially decaying component-dependent on the resonant frequency ω_o and quality factor 'Q', and a phase term also dependent on the resonant frequency.

$$E(t) \propto A\, e^{-j\omega_o} e^{-\omega_o t/2Q} \tag{3.1}$$

$$|E(\omega)|^2 \propto \frac{|A|^2}{(\omega-\omega_o)^2 + (\frac{\omega_o}{2Q})^2} \tag{3.2}$$

The square of the modulus of the Fourier Transform is proportional to the power transmitted, and its value in decibels is plotted as a function of frequency in Fig. 3-14. The nature of the curve is modified using the three parameters mentioned above, namely A, Q and ω_o. Though the theoretical curve was optimized through manipulation of the three parameters, it did not provide a sufficiently close fit to the experimental transmission curve observed. This led to the investigation of a condition where two modes staggered in frequency and differing in their Q's possibly with a phase shift between them were competing in the cavity space.

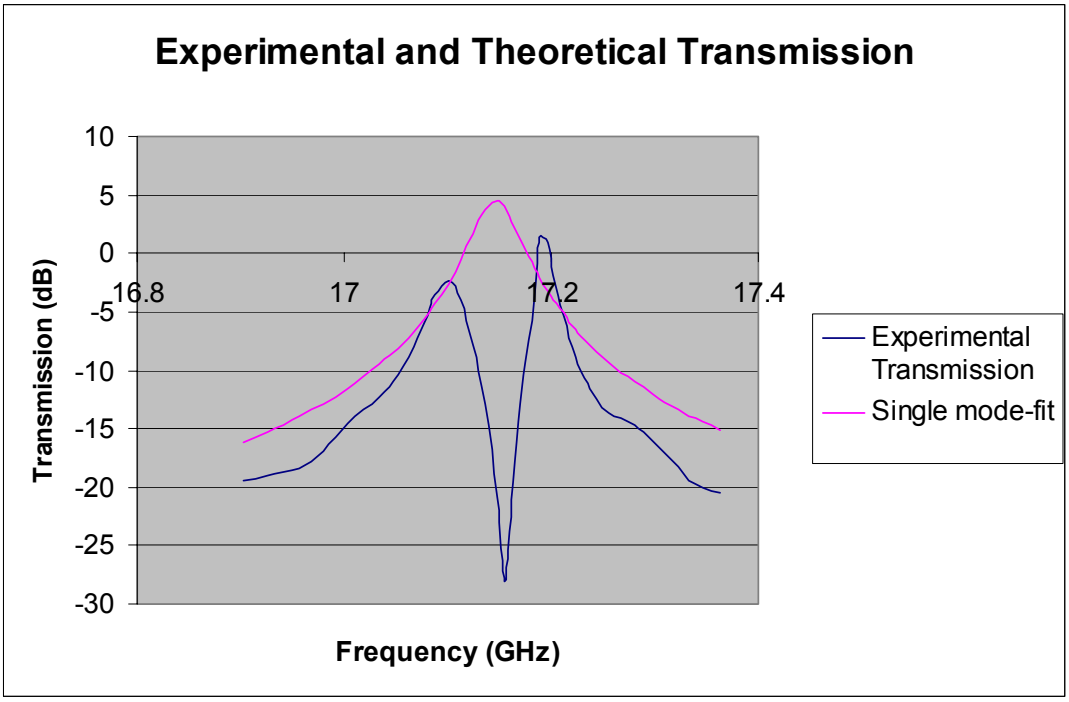

Figure 3-14: Experimental transmission and theoretical single frequency Fourier fit.

The electric fields of the 2 modes E_1 and E_2 are modeled with their respective amplitudes-A_1, A_2, quality factors-Q_1, Q_2 and resonant frequencies-ω_1, ω_2. Additionally the relative phase shift between the 2 terms is accounted for by the ϕ term. The electric field terms add up in the frequency domain, and the square of the modulus of the resultant field is proportional to the power transmitted through the cavity.

$$E_1(t) \propto A_1 e^{-j\omega_1} e^{-\omega_1 t/2Q_1} \qquad (3.3)$$

$$E_2(t) \propto A_2 e^{-j\omega_2} e^{-\omega_2 t/2Q_2} e^{j\phi} \qquad (3.4)$$

$$|E(\omega)|^2 = |E_1(\omega) + E_2(\omega)|^2 \qquad (3.5)$$

A 5-parameter optimization was carried out manually, using gridlines as reference points to ensure a close fit between the experimental curve (Fig. 3-16) and the Fourier

approximation (Fig. 3-15). The results of the best fit obtained are summarized in the Table 3-4.

	Mode 1	Mode 2
Resonant Frequency (GHz)	17.105	17.194
Quality Factor (Q)	450	700

Table 3-4: Theoretical estimate of the 2 modes present in the cavity. The relative phase shift ϕ is $-\pi/5.8$ between the 2 modes.

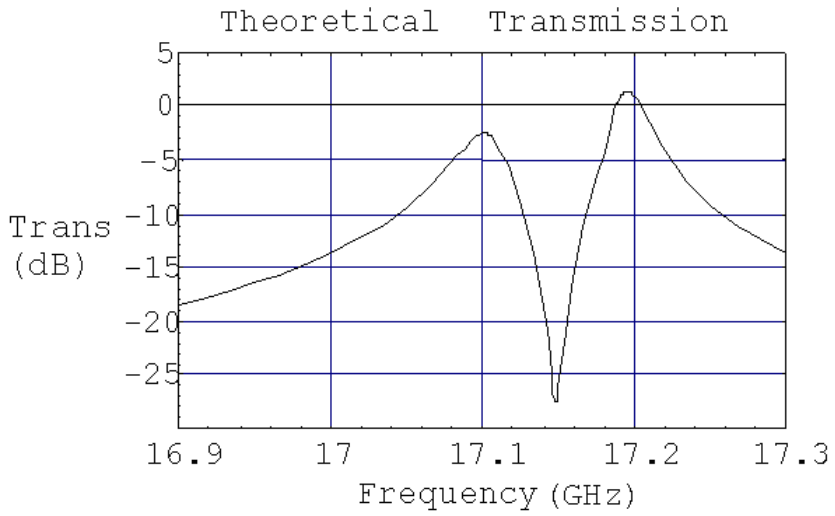

Figure 3-15: Theoretical dual frequency Fourier fit.

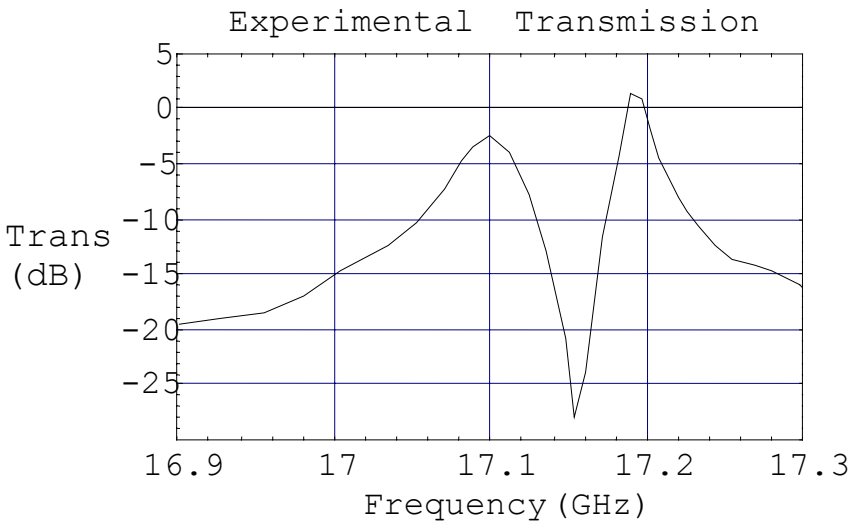

Figure 3-16: Experimental transmission curve exhibiting dual hump.

3.11 Investigation of causes leading to dual mode existence in the cavity

One hypothesis to explain the dual peak phenomenon in the cavity was the advent of eccentricity in the individual assemblies that constitute the cavity - i.e. the upstream and downstream inserts, the inner coax etc. However these parts were measured thoroughly on the Coordinate Measurement Machine (CMM) and were consistently observed to have eccentricity ranges below 0.2 mils. As the parts themselves were circular within machining tolerances, a relative shift or slop between the inner conductor and the inserts was thought to produce the undesirable effect observed experimentally. The misalignment could manifest itself in two ways and practically could be a combination of both - namely:

1. A radial offset between the inner conductor and the inserts, resulting in them having dissimilar axes of symmetry.

2. An axial offset of the inner conductor with respect to the inserts, resulting in a misalignment of the depressions on the inner and outer radial walls that constitute the cavity.

The difficulty in estimating the absolute error or misalignment was compounded by the fact that the downstream insert doses not make contact with the corresponding faceplate directly, but has a compressible O-ring sandwiched between them. Consequently all distances are to be referenced from the opposite faceplate where the insert makes direct physical contact with the faceplate of the micrometer gauge.

3.12 HFSS modeling of misalignments in the output cavity and housing

The HFSS cavity model was originally simulated as a quartered section (90 degree slice) of an azimuthally symmetrical structure. To accommodate a radial offset of the inner conductor relative to the outer housing, the model is mirrored into a half section. Starting with baseline data S_{21} transmission curve without any radial or axial offset (Fig. 2-10), the inner conductor is shifted by 2 mils along either the X or Y axes, with no alteration in the Z positioning. The entire structure is then analyzed to obtain the corresponding S_{21} plot (Fig. 3-17), which exhibits a prominent resonance at 17.08 GHz and a smaller peak at 17.155 GHz.

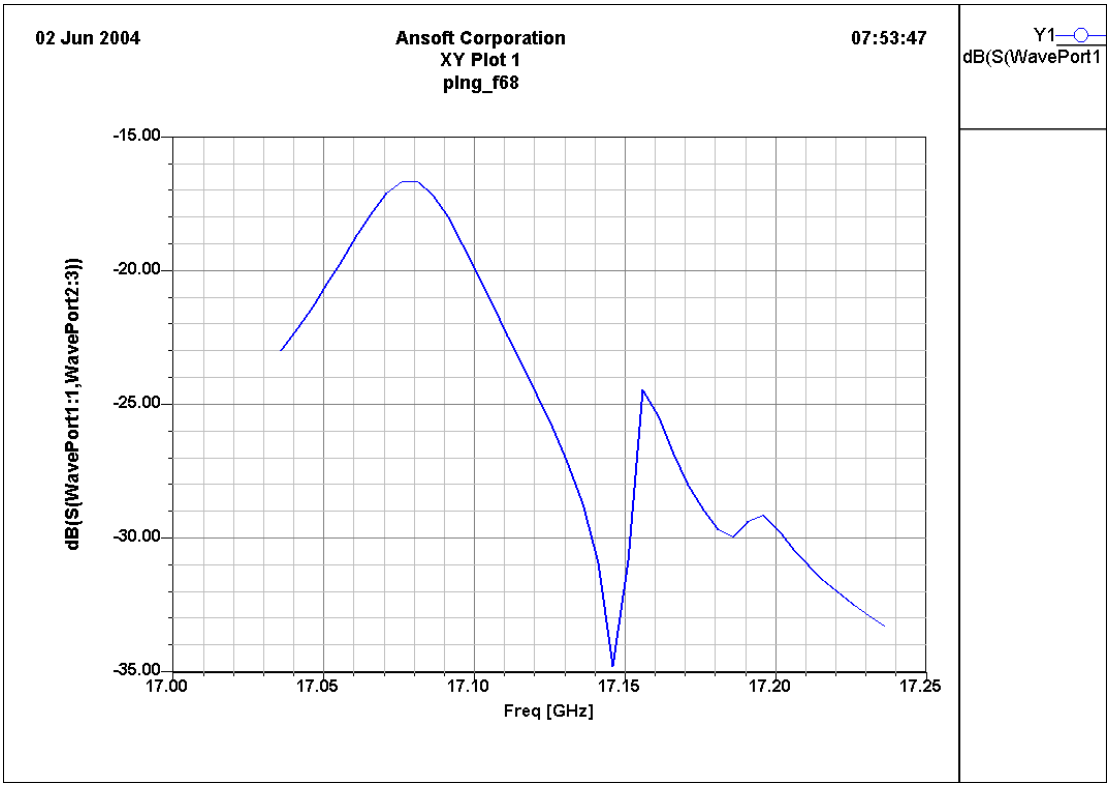

Figure 3-17: S_{21} transmission curve for 2 mil radial offset, peaks at 17.08 GHz and 17.155 GHz.

One additional variation studied in the simulation is to quantify the effect of a 45-degree rotation about the azimuth of the inner conductor, which would center one of the coupling apertures directly above the injection port. (In the original test configuration the metal strip between the coupling slots would be positioned directly below the coupling aperture) HFSS predicts the appearance of smaller local resonant peaks in the transfer curve as indicated in Fig. 3-18, in addition to a slight increase (~0.6dB) in the amplitude of the peaks when the aperture is centered under the injection port. Experimental data agrees quantitatively, with an increase of 0.79 dB in the amplitude of the primary resonant peak in this configuration.

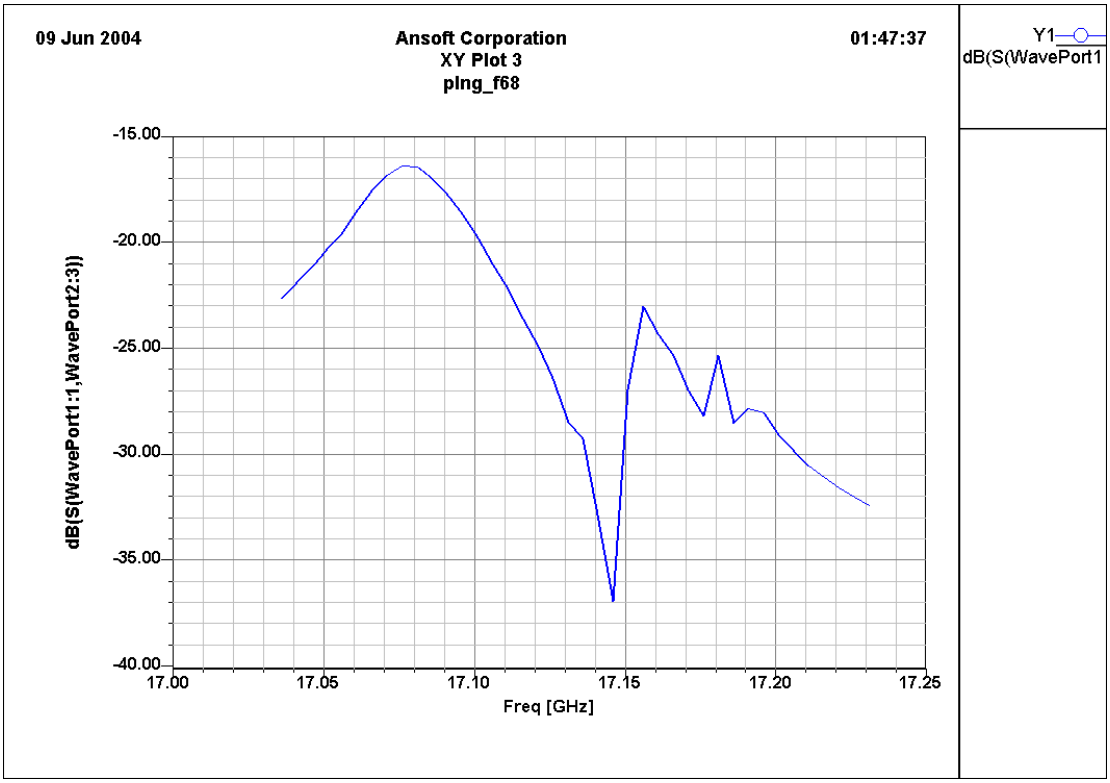

Figure 3-18: S_{21} transmission curve for 2 mil radial offset and 45 degree rotation of inner conductor, peaks at 17.07 GHz and 17.155 GHz.

To simulate the effect of an axial displacement between the inner coax and the outer conductor, the quarter symmetry section is again used to cut down on computation time. Keeping the X and Y position of the inner conductor as per the base line model constant, it is then offset by 1 mil axially along Z. This results in a misalignment of the changes in the radii of the inner and outer conductors that define the output cavity. The resulting S_{21} transmission curve is shown below in Fig. 3-19. The axial offset also results in a prominent downshifting in frequency of the two humps in the transmission curve.

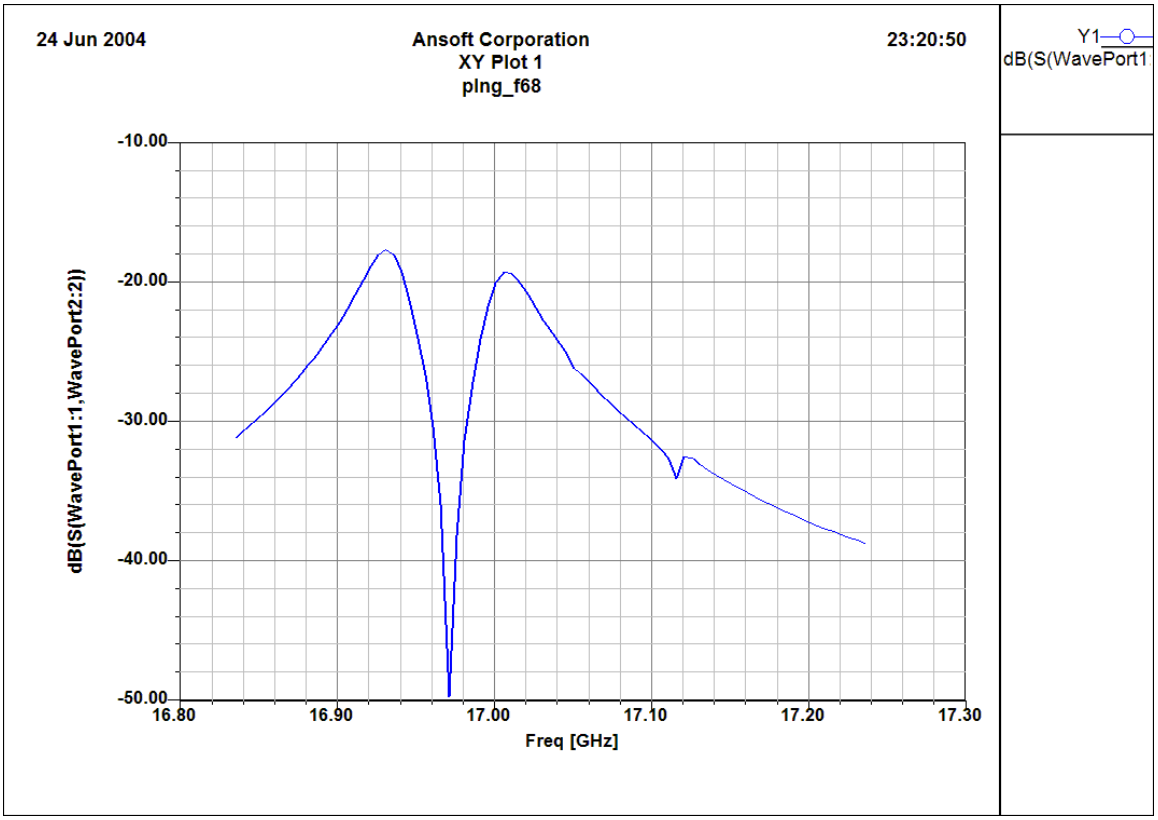

Figure 3-19: S_{21} transmission curve for 1mil axial offset between inner coax and outer conductor, peaks at 16.93 GHz and 17.01 GHz.

3.13 Experimental verification of cavity misalignments

To verify the effect of the radial offset experimentally, the inner conductor was shifted relative to the inserts by introducing a strip of 2 mil shim stock between the outer housing and the inserts. As the inner conductor itself is supported by the faceplates of the cavity housing at the two ends, this amounts to a 2 mil radial offset of the inner conductor with respect to the outer wall of the cavity. From Fig. 3-20 we see that the transmission curve closely resembles the simulated curves of Figs. 3-17

and 3-18, exhibiting the dual peak structure, with a prominent resonant peak centered at 17.09 GHz and a Q of 462.

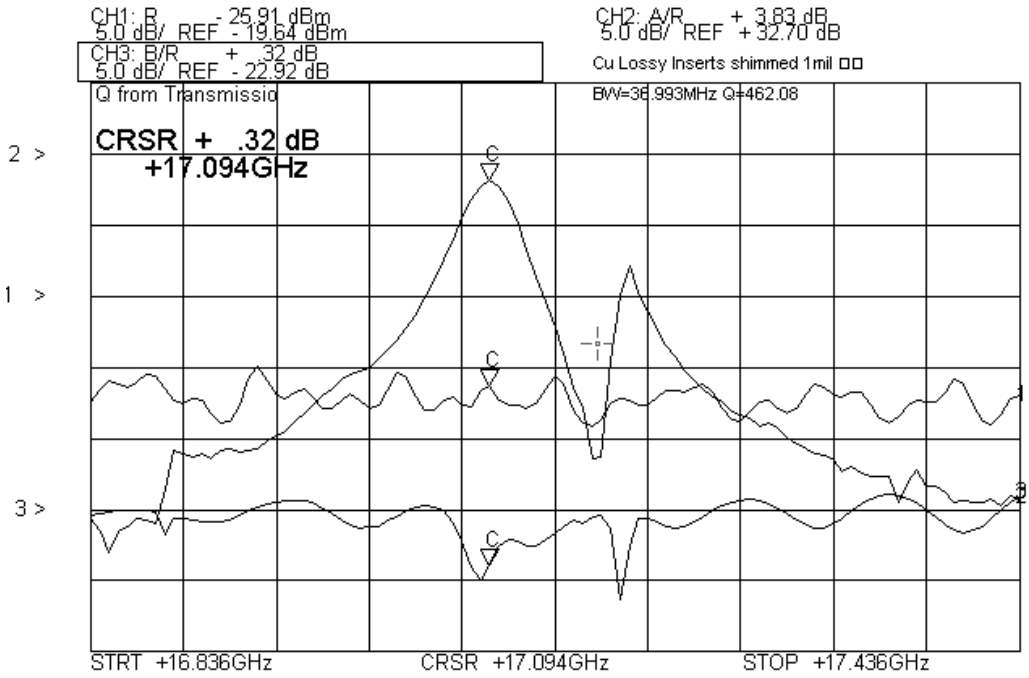

Figure 3-20: Experimental S_{21} transmission curve with inserts shimmed to mimic 2 mil radial offset, peaks at 17.094 GHz and 17.183 GHz.

Figures 3-21 and 3-22 illustrate the electric field distribution in a slice across the center of the cavity and a longitudinal slice respectively. The TE_{021} cavity mode, though visible, lacks perfect azimuthal symmetry.

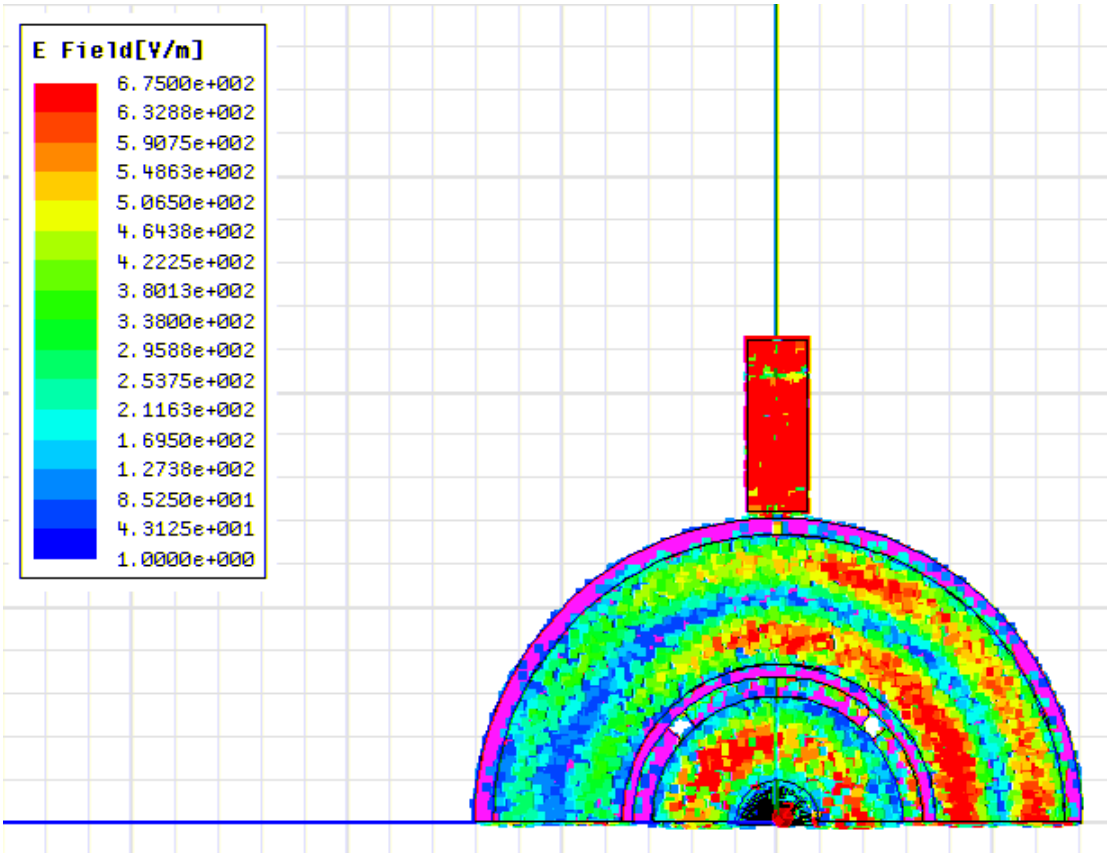

Figure 3-21: E-field distribution across cavity center for 2 mil radial offset.

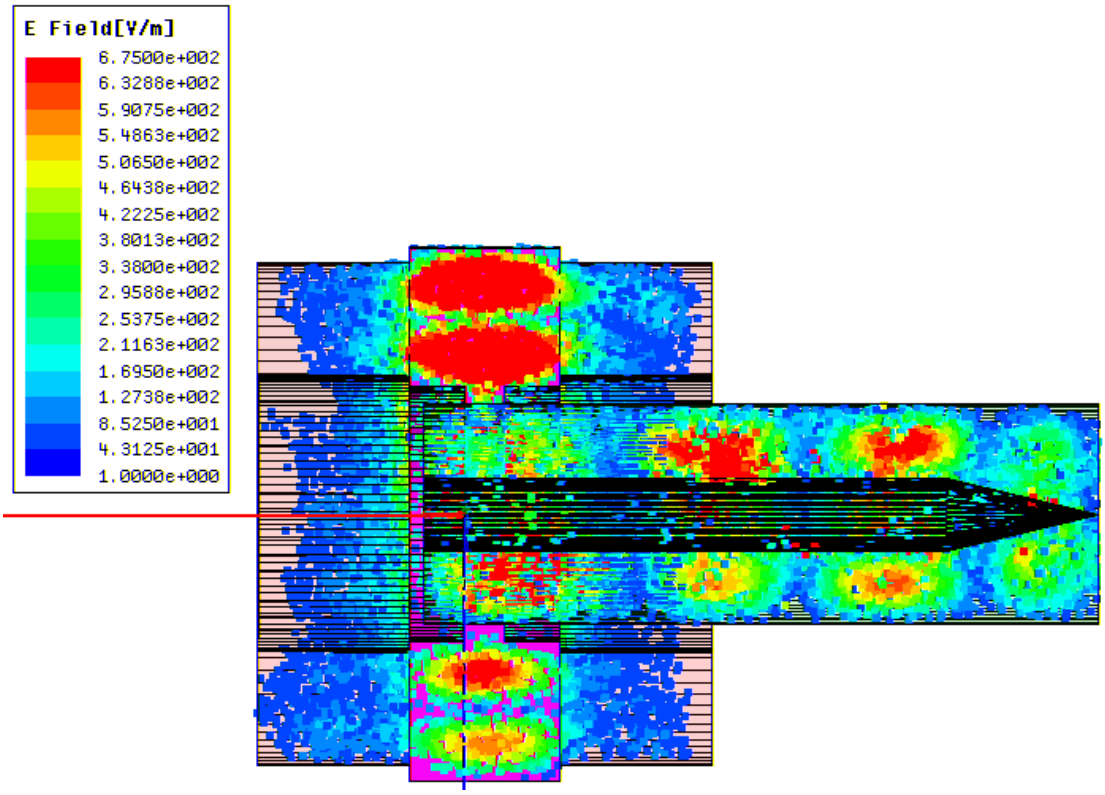

Figure 3-22: E-field distribution in a longitudinal slice of the cavity structure for 2 mil radial offset.

In addition to simulating the transmission curve of the cavity for a 2 mil radial offset, the procedure was repeated for a radial offset of 4, 6, and 8 mils as well. This was to gain information about the behavior of the spurious mode with regards to its resonant peak and relative amplitude when compared to the prominent resonant peak. Practically though, simulation of radial perturbation beyond 4 mils would be unnecessary as there was insufficient slop between the inserts and the cavity housing to accommodate a radial offset exceeding that value. From Fig. 3-23 we see that the spurious mode in the 2 mil radial offset case is below the main resonance by 6.5 dB,

which agrees quantitatively with amplitude difference experimentally observed in Fig. 3-20.

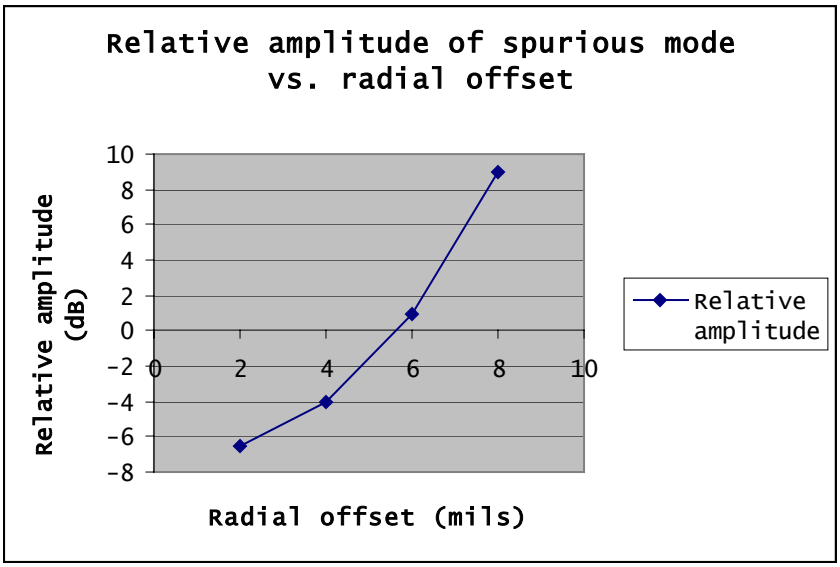

Figure 3-23: Theoretical (HFSS) relative amplitude of spurious mode w.r.t. amplitude of prominent resonance peak as a function of radial offset.

An axial offset of the inner conductor that will misalign the inner and outer cavity walls, can be mimicked by taking advantage of the compressibility of the O-ring seal on the downstream faceplate. As the inner conductor is rigidly supported between the faceplates, shim stock that would compress the inserts towards the O-ring seal were inserted to produce an offset of 1 mil. Alternately, by CMM measurements it was found that the same effect could be replicated by interchanging the positions of the upstream and downstream inserts. The experimental transmission curve obtained in this configuration is shown in Fig. 3-24 and it closely resembles the transmission curve of Fig. 3-19, predicted by HFSS.

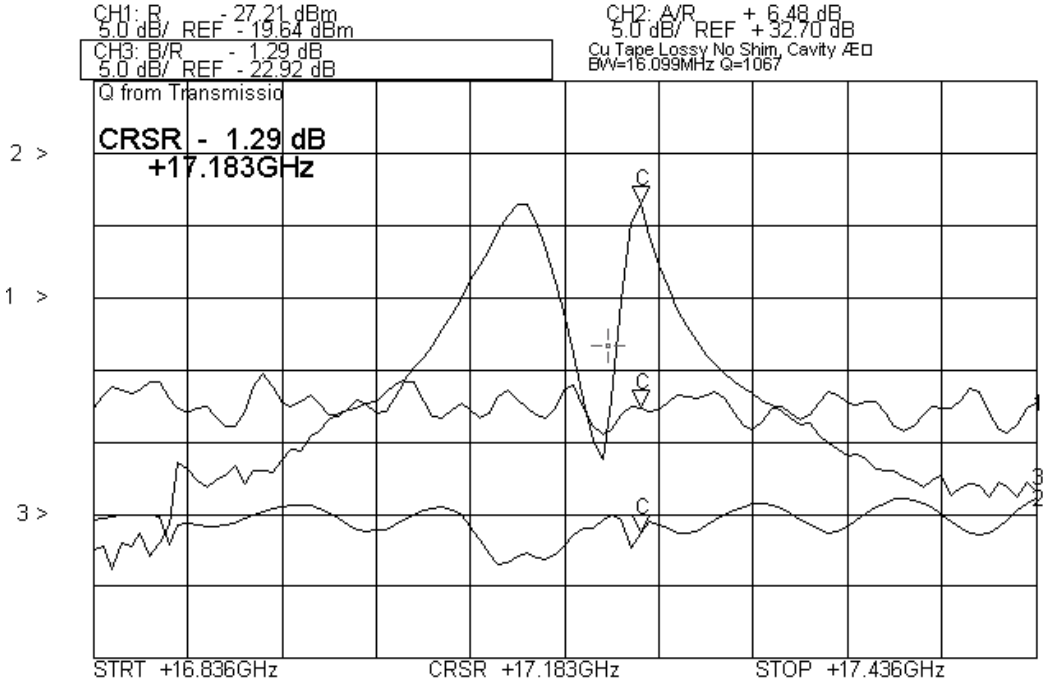

Figure 3-24: Experimental S_{21} transmission curve with upstream and downstream inserts interchanged to mimic axial perturbation/displacement, peaks at 17.112 GHz and 17.183 GHz.

The distortion produced in the electric field structure of the TE_{021} cavity mode is much more pronounced, as is evident from the cavity center slice (Fig. 3-25) and the longitudinal slice (Fig. 3-26).

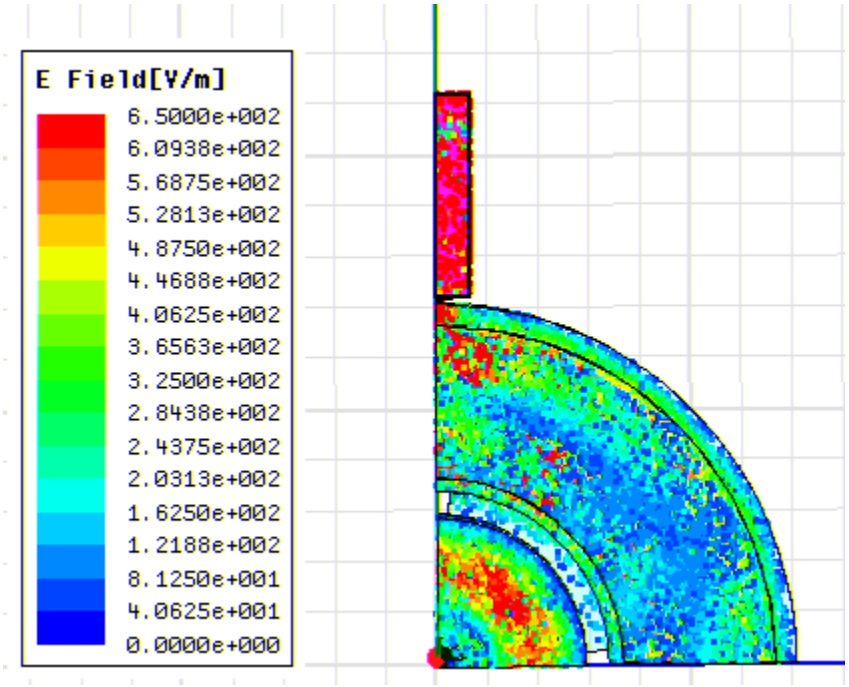

Figure 3-25: E-field distribution across cavity center for 1 mil axial offset.

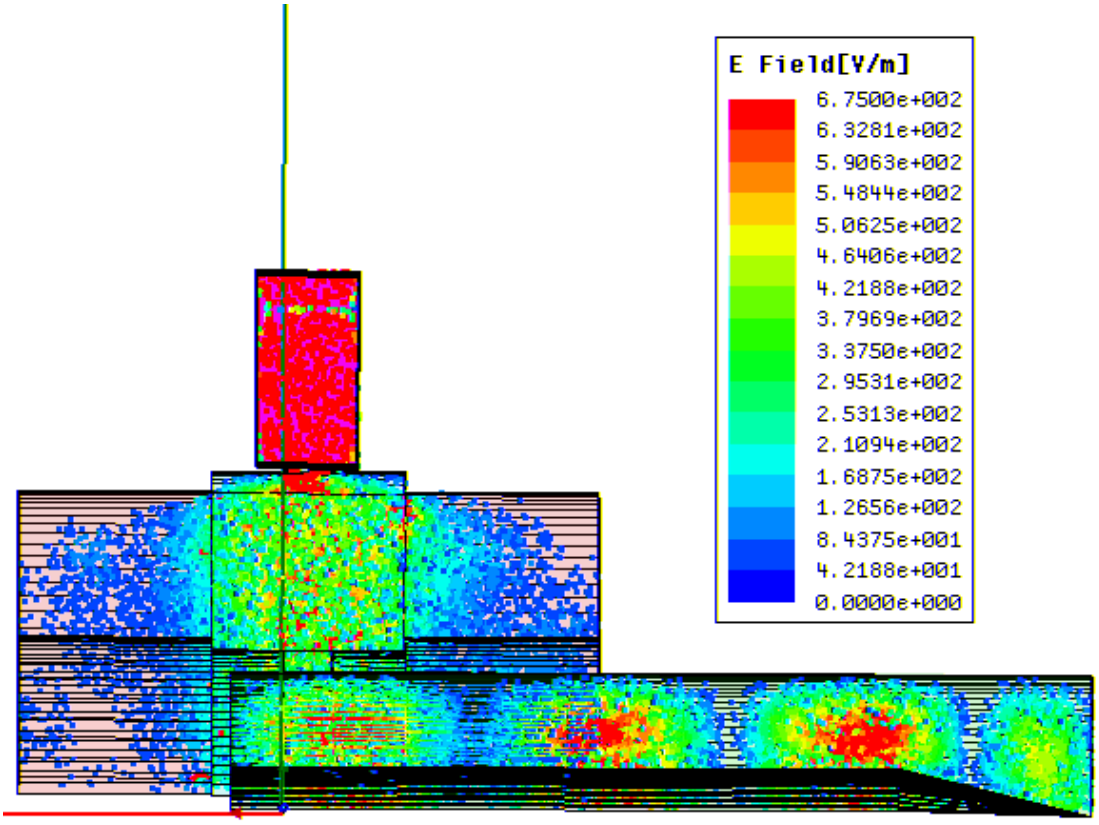

Figure 3-26: E-field distribution in a longitudinal slice of the cavity structure for 1 mil axial offset.

3.14 Corrected cavity performance

Having experimentally verified the radial and axial offsets independently, the slop in the cavity structure (which in all likelihood would possess some combination of the 2 misalignments) is compensated for by using 0.5 mil shim stock between the cavity housing and the inserts, and adjustment of the inner conductor. The transmission curve produced by this corrected cavity is shown in Fig. 3-27. It exhibits a resonant peak at 17.112 GHz with a Q of 458. The theoretical and cold test performance of this cavity are compared to that of the current output cavity present in the system in Table 3-5.

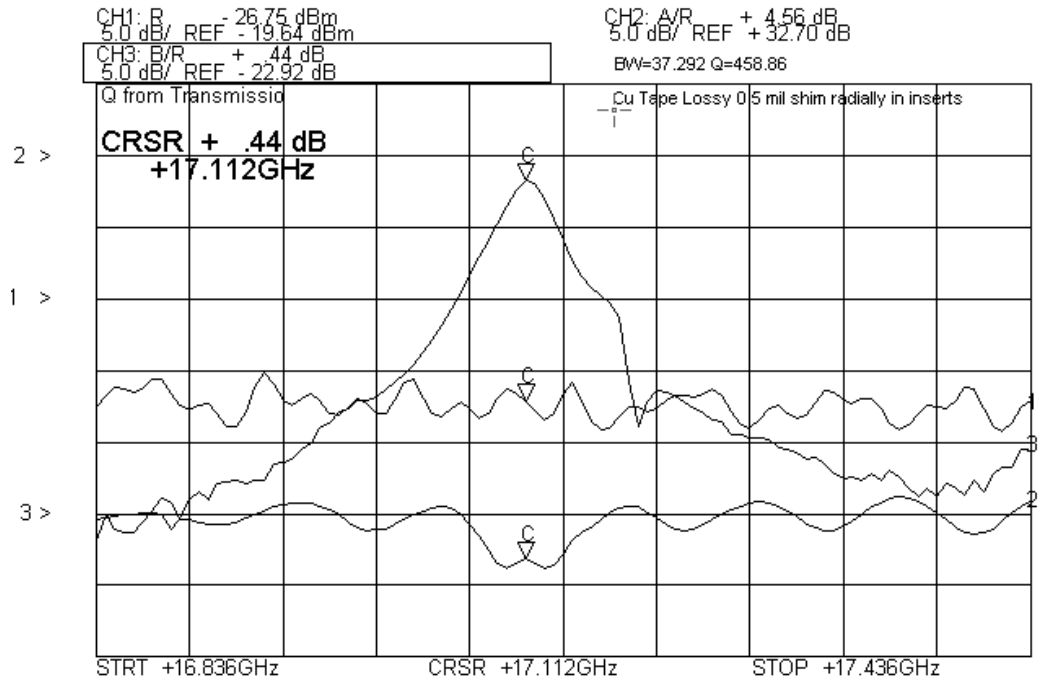

Figure 3-27: Experimental S_{21} transmission curve with both axial and radial offsets compensated, resonant peak at 17.112 GHz.

	Radial extraction output cavity (experimental)	Radial extraction output cavity (HFSS)	Current axial extraction output cavity
Resonant frequency (GHz)	17.112	17.08	17.115
Quality Factor (Q)	458	354	310

Table 3-5: Comparison of radial and axial extraction output cavity performance.

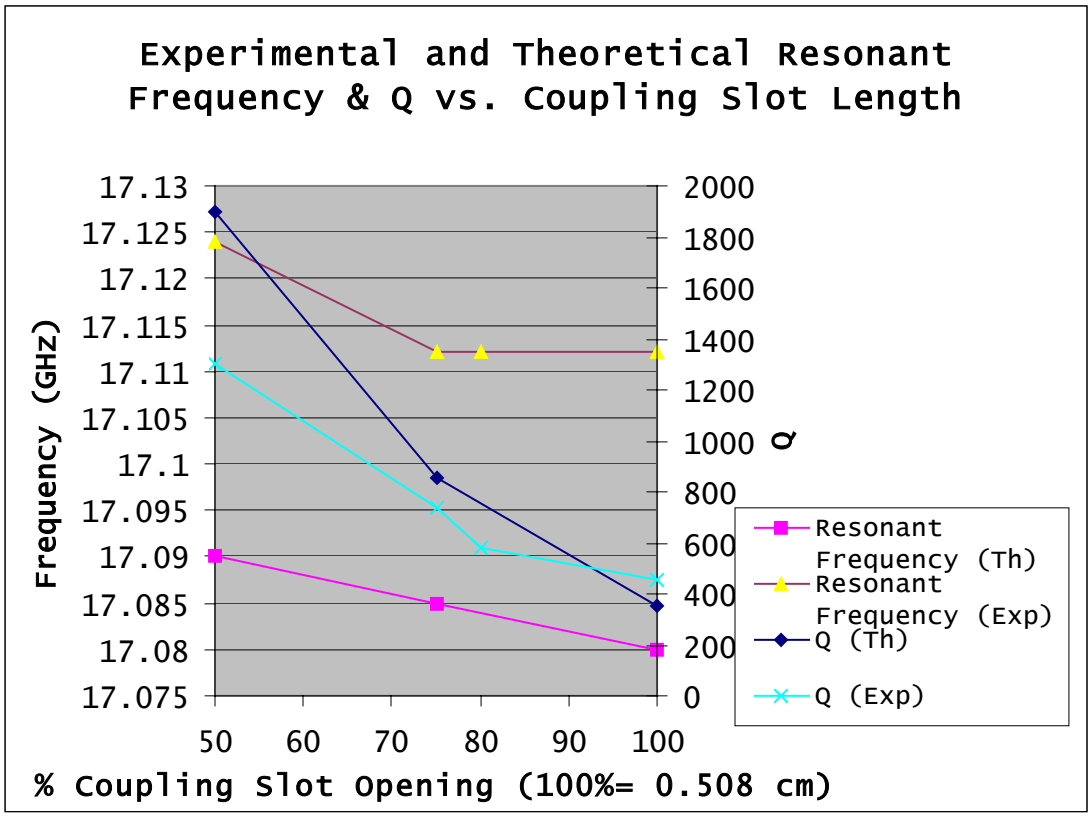

Figure 3-28: Variation of resonant frequency and Q as a function of slot length for the corrected cavity.

The effective coupling slot length is progressively reduced from its maximum of 0.508 cm to about 50 % of its original length using a strip of copper tape to mask the slots. The resonant frequency and Q are then plotted as a function of the slot opening (Fig. 3-28). The same procedure is simulated in HFSS to obtain experimental trends in the resonant frequency and Q. In the corrected cavity the cold test Q of 458 observed with the slots completely open is much closer to the predicted value of 354. More significantly the experimental Q in the corrected cavity rises to about 1200 with the coupling slots closed 50 %, which is in keeping with the theoretical estimate. In case of the poorly aligned cavity with lossy material till the lip (Fig. 3-11), the Q

barely reaches 440 even with the slots closed 75 %. Thus, although the lossy material suppresses the spurious mode, producing the desired single hump transmission curve, it contributes to higher losses in the drift regions, which forces the Q well below the theoretical value predicted by HFSS. The experimental resonant frequency plot shows an upshift of around 30 MHz as compared to the theoretical curve.

Chapter 4: Conclusions

This thesis thus characterizes the design performance of the radial extraction output cavity and presents it as a viable solution to replace the axial extraction output cavity currently in the system. Finer points on the operation of the cavity, such as the positioning of dielectrics in the drift regions, are revealed in the cold testing. It also gives clear guidelines on the limits of design tolerances that can be introduced in the fabrication process without adversely affecting cavity performance. The electromagnetic parameters of the cavity (resonant frequency, Q, etc) are acutely sensitive to any misalignment between the inner conductor and the inserts that constitute the cavity. A radial offset of 2 mils (or greater) between the inner and outer conductors, produces a dual peak transmission curve, and a moderately distorted field structure of the expected TE_{021} coaxial mode. The difference between the amplitudes of the resonant peaks is however in excess of 5 dB, allowing for sufficient discrimination between the two. The effect of a one mil axial misalignment between the inner conductor and the inserts is more pronounced. It is characterized by 2 competing modes, a distorted field structure of the TE_{021} mode, and nearly equal amplitude of the 2 resonant peaks. The experimentally determined resonant frequency of the cavity compensated for radial and axial misalignments is 17.112 GHz, which is 32 MHz higher than the theoretical HFSS predicted frequency of 17.08 GHz. The corresponding cold test measured Q is 458 which is higher than the

theoretical Q by about 100. The simulation procedure to extract cavity parameters from HFSS is inherently difficult, and hence its predicted cavity performance should not be treated as an exact result. They serve as guidelines for the design of a cold test piece, which can subsequently be fine-tuned to obtain exact cavity dimensions for a desired resonant frequency and Q.

This cavity should enable the system to be zero drive stable, permit extraction of the amplified microwaves from the gyroklystron in the TE_{01} circular mode, and obviate the need for large reduction in the output waveguide dimensions or a ripple wall mode converter section. Thus it would be ideally suited to inject directly into the compact TE_{01} circular to TE_{20} rectangular mode converter in the HRC accelerator structure feed chain.

References

[1] V. L. Granatstein and W. Lawson, "Gyro-Amplifiers as Candidate RF Drivers for TeV Linear Colliders," IEEE Trans. Plasma Sci. 24 [3], 648-664 (1996).

[2] P. E. Latham, W. Lawson, and V. Irwin, "The Design of a 100 MW, Ku-Band Second Harmonic Gyroklystron Experiment," IEEE Trans. Plasma Sci. 22, 804-817 (1994).

[3] J. Cheng, X. Xu, W. Lawson, J. P. Calame, M. Castle, B. P. Hogan, and V. L. Granatstein, G. S. Nusinovich, and M. Reiser, "Experimental Studies of a High-Power, X-Band, Coaxial Gyroklystron," IEEE Trans. Plasma Sci. 27, 1175-1187 (1999).

[4] J. Haimson and B. Mecklenburg, "A Linear Accelerator Power Amplification System for High Gradient Structure Research", in *Proc. Advanced Accelerator concepts*, pp. 1003-1013, (1998).

[5] I. Spassovsky, E. S. Gouveia, S. P. Tantawi, B. P. Hogan, W. Lawson, and V. L. Granatstein, "Design and Cold-Testing of a Compact TE_{01} -> TE_{20} Mode Converter", IEEE Trans. Plasma Sci. 30, 787-793 (2002).

[6] W. Lawson, M. Esteban, H. Raghunathan, B. Hogan, and K. Bharathan, "Ripple-Wall Mode Converters for High Power Microwave Applications", to be published in IEEE Trans. Microwave Theory Tech.

[7] J.P. Anderson, “The Advanced-Concept Gyroklystron Design”, Master of Science Thesis, University of Maryland, 1997.

[8] E. S. Gouveia, “Development of a Four Cavity Second-Harmonic Gyroklystron as Driver for a Linear Accelerator”,Ph.D Dissertation, University of Maryland College Park, 2004.

[9] W. Lawson, "Theoretical Evaluation of Nonlinear Tapers for a High-Power Gyrotron," IEEE Trans. Microwave Theory Tech. 38, 1617-1622 (1990).

[10] J. Calame and W. Lawson, "A Modified Method for Producing Carbon Loaded Vacuum Compatible Microwave Absorbers from a Porous Ceramic," IEEE Trans. Electron Dev., Part 2, 38, 1538-1543 (1991).

[11] W. Lawson, J. Cheng, M. Castle, B. Hogan, V. L. Granatstein, M. Reiser, and G. P. Saraph, "High-Power Operation of a Three-Cavity X-Band Coaxial Gyroklystron," Phys. Rev. Lett. 81, 3030-3033 (1998).

[12] Emerson & Cuming Microwave Products, ECCOSORB-BSR Specification Sheet, Revision 11/12/02.

[13] Elisra Electronics Systems Ltd., Microwave Division.

[14] ANSOFT High Frequency Structure Simulator, v 9.1.